Citation: Timón-Sánchez, S.M., López-Moro, F.J., Romer, R.L., Rhede, D., Fernández-Fernández, A., Moro-Benito, C., 2019. Late-Variscan multistage hydrothermal processes unveiled by chemical ages coupled with compositional and textural uraninite variations in W-Au deposits in the western Spanish Central System Batholith. *Geologica Acta, Vol.17.1, 1-19.*
DOI: 10.1344/GeologicaActa2019.17.1

Late-Variscan multistage hydrothermal processes unveiled by chemical ages coupled with compositional and textural uraninite variations in W-Au deposits in the western Spanish Central System Batholith

S.M. Timón-Sánchez[1] F.J. López-Moro[2] R.L. Romer[3] D. Rhede[3] A. Fernández-Fernández[2] C. Moro-Benito[2]

[1]Instituto Geológico y Minero de España, IGME
Plaza de la Constitución 1, Planta 3ª, 37001 Salamanca, Spain. Timón-Sánchez E-mail: s.timon@igme.es

[2]Departamento de Geología, Universidad de Salamanca
Plaza de Los Caídos s/n, 37008 Salamanca, Spain. López-Moro E-mail: fjlopez@usal.es
Fernández-Fernández E-mail: aff@usal.es
Moro-Benito E-mail: cmoro@usal.es

[3]Deutsches GeoForschungsZentrum, GFZ
Telegrafenberg 14473 Postdam, Germany. Romer E-mail: romer@gfz-potsdam.de
Rhede E-mail: dieter.rhede@gfz-potsdam.de
Moro-Benito E-mail: cmoro@usal.es

ABSTRACT

The scheelite skarn from Los Santos and the W-Au veins from El Cabaco district, located in the Spanish Central System Batholith (SCSB), are some of the best-known tungsten ore deposits in Spain. Uraninite is an accessory mineral in both deposits, which underwent several hydrothermal flow events. Chemical and textural characteristics as well as electron microprobe U-Th-Pb uraninite chemical data from the different stages of the skarn and the vein-type mineralizations are presented here. Based on these data the uraninite was able to be classified into two groups. Group I uraninite has an octahedral habit and occurs as inclusions in K-feldspar relicts of the leucogranite related to Los Santos skarn formation. It shows high Th (6.95 to 8.51wt.% ThO_2) and high Rare Earth Elements (REEs) contents (0.55 to 1.38wt.% $\sum REE_2O_3$). Group II uraninite occurs i) associated to El Cabaco granite, in a greenish selvage-style greisen and its reddish envelope and in the mineralized rimming quartz veins and ii) in Los Santos high temperature endoskarn and anorthite skarn, where it is associated with U-rich mica. This uraninite type has lower Th and $\sum REE_2O_3$ contents than Group-I uraninite. The mineral chemistry and the assemblage and textural relationships suggest that Group-I uraninite is magmatic and the attained U-Th-Pb chemical age of 300±4Ma is interpreted as the magmatic age of the skarn-forming aplite granites in the western part of the SCSB. Group-II uraninite includes two events: i) a hydrothermal uraninite, which yields an age of 295±2Ma, dates a strong-alkali mobilization and early tungsten deposition and ii) a later hydrothermal processes, around 287±4Ma, that resulted in sulfides and late scheelite precipitation and widespread silicification. Finally, the gold deposition is younger than this silicification according to textural criteria. Therefore, W-Au deposits in the western part of the SCSB were formed by superposition of several processes that took place some 15Ma after the skarn-forming granite crystallized. Comparable W, W-Au and U deposits in the Variscan orogenic belt show a similar timing of hydrothermal events, suggesting that the hydrothermal history was controlled by large-scale Late-Variscan tectonic processes.

KEYWORDS | **Uraninite. U-Pb dating. W-Au deposits. Spanish Central System Batholith. Variscan belt.**

INTRODUCTION

Uraninite is widely used for chemical dating as its high contents of Pb and U are easily measured by electron microprobe. Uraninite chemical dating may provide precise ages (*e.g.* Alexandre and Kyser, 2005; Finger *et al.*, 2017; Förster, 1999; Förster *et al.*, 2012; Kempe, 2003; Pal and Rhede, 2013; Romer *et al.*, 2007; Votyakov *et al.*, 2013), especially if silicate minerals shield uraninite from later oxidation, which would make uranium mobile. The combination of chemical dating with detailed textural and chemical studies of uraninite may provide good constraints on the age and the history of multiple hydrothermal metal redistribution (*e.g.* Pal and Rhede, 2013).

Magmatic and hydrothermal mineralization and associated altered rocks in the Spanish Central System Batholith (SCSB) include scheelite, wolframite and cassiterite mineralization in sulfide veins and greisens (Martín-Crespo *et al.*, 2004; Vindel *et al.*, 2000), Sn-W skarns (Casquet and Tornos, 1984), episyenites (Caballero *et al.*, 1993), and scheelite sulfide-rich veins (Tornos *et al.*, 1993). At many locations, several different types of mineralization occur in sequence. Without isotopic dating, it is a priori unclear whether these different stages of mineralization are different expressions of the same general process and, thus, belong to one single event, or they are related to several different unrelated events. In either case, isotopic dating of particular mineral assemblages provides key information, as it makes possible to link mineralization to heat sources and tectonic events that operate on a local and regional scale. We study two W±Au±U deposits of the SCSB, *i.e.* Los Santos scheelite skarn and El Cabaco vein and greisen mineralization. Both deposits show uraninite associated with several mineral assemblages (López-Moro *et al.*, 2007; Timón, 2008), making it possible to date different events of hydrothermal activity.

Los Santos scheelite skarn is a major tungsten deposit currently operated by Almonty Industries Inc. It is a mesozonal, calcic and reduced tungsten-bearing skarn deposit (Timón *et al.*, 2007; Timón and Moro, 2007; Timón, 2008; Tornos *et al.*, 2008) that evolved from a magmatic to a hydrothermal system. The hydrothermal system has been assumed to be distinctly younger than Variscan magmatism (Timón *et al.*, 2009).

El Cabaco deposit consists of gold-and wolframite-scheelite-bearing sulfide-rich veins that may form quartz veins and stockwork-selvage-style greisen (López-Moro *et al.*, 2007). Geochronological and structural data and the nature of fluids associated to this deposit suggest that the hydrothermal activity is distinctly younger than the emplacement of the granitic rocks (Antona, 1991; Antona *et al.*, 1994; González-Sánchez, 2003). For instance, muscovite from the salbands yielded a K-Ar age of 256±5Ma (Antona, 1991).

In this contribution we present chemical, textural and chemical age data of uraninite hosted by different metasomatic rocks in two contrasted W-Au deposits, namely Los Santos and El Cabaco deposits, which have undergone several events of hydrothermal overprint. We discuss the processes related to the formation of the different uraninite types and discuss their age in the context of other W-Au hydrothermal deposits from the SCSB and the Variscan orogen.

GEOLOGICAL SETTING

The studied deposits are located in the Central Iberian Zone (CIZ), which is part of the Iberian Massif, an internal domain of the Variscan belt (Fig. 1A). In the CIZ, the Proterozoic Gondwana basement is overlain by mainly siliciclastic sedimentary rocks that form a passive margin sequence (*e.g.* Fernández-Suárez *et al.*, 2002; Gutiérrez-Alonso *et al.*, 2005). The Precambrian-Cambrian metasedimentary sequence, known as the Schist-Greywacke Complex, consists of two major units: the Lower Unit, a succession of shales and sandstones, and the Upper Unit, which predominantly includes pelitic rocks and comprise two formations: Monterrubio and Aldeatejada formations (Díez Balda, 1986, 1980). The Monterrubio Formation (Fm.) comprises about 2000m of slates with intercalations of sandstones, conglomerates, and volcanoclastic rocks. The conformable overlying Aldeatejada Fm. is 1600m-thick and consists of slates with intercalations of laminated black shales and phosphorite conglomerates. The Aldeatejada Fm. is overlain by the Lower Cambrian Tamames Sandstone, the Tamames Limestone, and the Endrinal Shale. Above a first-rank discordance, these rocks are overlain by Ordovician to Devonian sedimentary rocks, which are exposed in NW-SE trending synclines.

The igneous rocks of the studied area are part of the SCSB (Fig. 1B), one of the most extensive and well-exposed granitoids in the Iberian Variscan belt. Granodiorites and monzogranites constitute more than 90% of the intrusive rocks, whereas the remaining 10% consist of basic and intermediate rocks, all of them defining a typical K-rich calc-alkaline association and outcropping in restricted locations (Moreno-Ventas *et al.*, 1995). The tectono-metamorphic evolution of the northern half of the CIZ includes four main phases of ductile deformation (Díaz-Alvarado *et al.*, 2013 and references therein): D_1 (upright and E-vergent folds coupled with contractional deformation), ~360–337Ma; D_2 (extensional detachments), ~337–316Ma; D_3 (upright folds and a new extensional episode), ~316–300Ma; and D_4 (upright folds and shear bands only described for the eastern part of the Spanish Central System (SCS)). Dating of zircon from Variscan granitoids reveals that most magmatism in the western part of the SCS occurred during the D_3 phase (309 to 303Ma) (Bea *et al.*, 2004; Díaz Alvarado *et al.*, 2013; Gutiérrez-

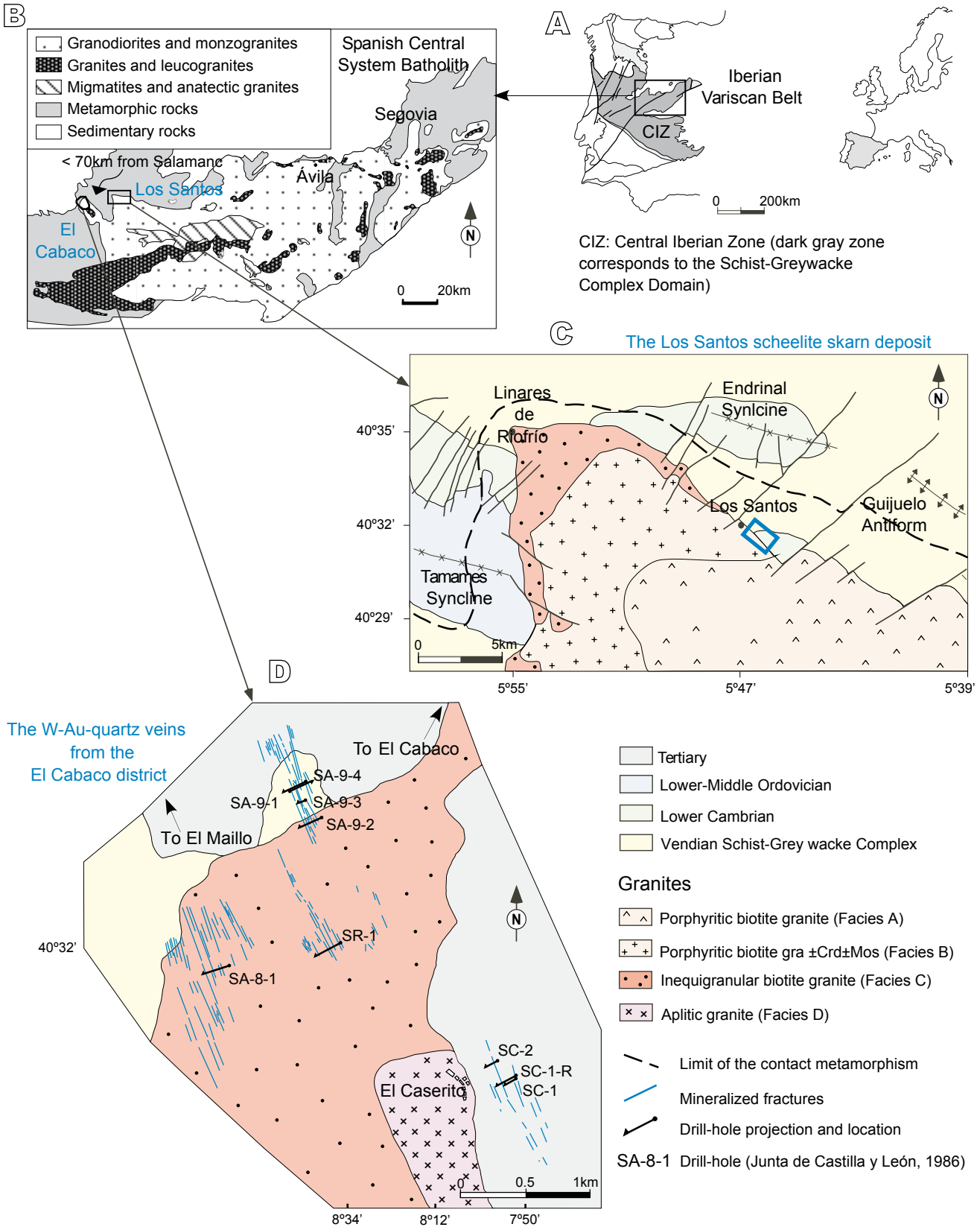

FIGURE 1. A) Location of the Central Iberian Zone (CIZ) within the Variscan belt. B) Study areas in the northwest termination of the Spanish Central System Batholith (SCSB) (modified from Carnicero, 1983 and Bea *et al.*, 1999). C) Geologic setting of Los Santos scheelite skarn deposit (map from Yenes *et al.*, 1999). D) Geological sketch map of El Cabaco district with the location of the mineralized fractures and the drill-hole projection (Junta de Castilla y León, 1986).

Alonso *et al.*, 2011; Valle Aguado *et al.*, 2005; Zeck *et al.*, 2007). In the eastern sector of the SCS, granites show a similar structural relation, but seem to be slightly younger (305–298Ma, Orejana *et al.*, 2012).

In La Alberca-Béjar granitic area (Fig. 1C, D), four texturally and mineralogically contrasting granite types occur; A: porphyritic biotite granite; B: porphyritic biotite±cordierite±muscovite granite; C: inequigranular biotite granite; and D: fine-grained granite and aplites (*e.g.* Ugidos *et al.*, 1990). Rocks of the porphyritic facies A and B are dominantly biotite monzogranites with a higher content of cordierite and some muscovite in facies B rocks. In contrast to the rocks of the porphyritic facies, the facies C rocks have fewer alkali-feldspar megacrysts and less cordierite. Apatite, zircon, monazite and ilmenite are minor constituents in this granite type. Uraninite is rare and generally related to samples with a superimposed albitization (López-Moro *et al.*, 2007). Facies D was identified at the scale of the mine. The grain size of these rocks is finer than for rocks of the other granite types and alkali-feldspar megacrystals are missing, biotite is less abundant and cordierite, andalusite, muscovite, apatite, zircon, monazite and ilmenite are minor constituents (Yenes, 1996). Spatial relations between different granite facies indicate that porphyritic granites are younger than facies C, as the former enclose enclaves of facies C rocks. The gradual contacts between porphyritic granites (facies A and B) suggest a limited time span between the emplacement of these two facies. Similarly, rocks of granites facies C and D show gradual contacts. Actually, granites of facies C and D may be related via differentiation (Ugidos *et al.*, 1990).

Facies B and D granites occur in Los Santos skarn, but only facies D granite seems to be related to the formation of scheelite skarn, as fresh granite grades into endoskarn-type alteration with the development of calcic plagioclase and clinopyroxene (Timón *et al.*, 2009) (Fig. 1C). W-Au-quartz veins of El Cabaco district, in contrast, are hosted in facies C and D granites (Fig. 1D).

EL CABACO AND LOS SANTOS ORE DEPOSITS

W-Au-quartz veins from El Cabaco ore deposit

El Cabaco ore deposit is located in a NW-SE trending antiformal structure composed of Variscan granites at the core (facies C and D) and pelitic hornfels and metasedimentary rocks of the Monterrubio Fm. in the external parts. The entire area is discordantly overlain by Neogene sediments. El Cabaco deposit includes four steeply NE-dipping, SE to SSE striking swarms of quartz-veins (Fig. 1D). The thickness of the quartz-veins varies from 2mm up to 40cm, with most veins falling in the range of 2 to 10cm-width. These mineralized quartz-veins are hosted in the Variscan granitoids (facies C and D) and in rocks of the Monterrubio Fm. Quartz-veins in granitoids commonly show abundant muscovite that forms selvage-style greisen, which typically are enveloped by a reddish K-feldspar-enriched rim (due to hematite microinclusions) with traces of new albite and chloride, which are typical features of episyenites. Voids that formed during episyenitization were later filled by secondary silicification. Rare alkali-feldspar veins commonly do not show alteration haloes in the host rock. Quartz-veins hosted in the metapelites of the Monterrubio Fm. typically show a selvage of tourmaline with sulfides (mainly pyrrhotite). Quartz veins show evidence of a complex geological history with repeated openings and closings, and healing by quartz and carbonates. Basically, four types of ore assemblages can be distinguished in these vein swarms (Fig. 2): i) scheelite±wolframite±molibdenite±uraninite deposition (oxide stage) during the feldspatization/albitization process; ii) As-Fe-S deposition (sulfide stage), with scheelite and uraninite during the main silicification (milky quartz, Q_1) stage. The sulfide stage represents the most important mineralization by volume. Traces of native gold (Ag_{06-12}), tellurosulfides, native Bi and bismuthinite, which occur as very small drops in arsenopyrite, may be associated with this deposition event; iii) a main gold stage,

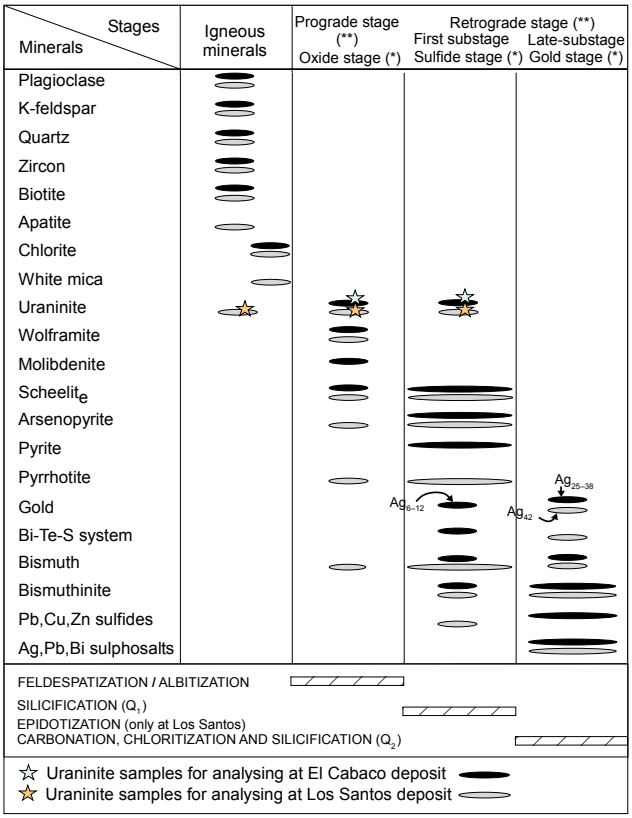

FIGURE 2. Paragenetic sequence of minerals, stages (*: stages distinguished at El Cabaco; **: stages distinguished at Los Santos) and main alterations present in both ore districts.

which includes electrum (Ag_{25-38}), base-metal sulfides, Bi-tellurides, tellurides and sulphosalts that preferably occur in fractures in arsenopyrite. This assemblage is related to carbonation, chloritization and silicification (clear quartz, Q_2); iv) a supergene stage, involving Ag-enriched electrum (Ag_{81}), bismite, Sb-uytenbogaardite and marcasite (Moro *et al.*, 2007).

Uraninite is restricted to greenish selvage-style greisen and its reddish envelope but is absent in the core of the quartz-veins. In these quartz-vein envelopes, uraninite is hosted by plagioclase, muscovite or quartz, whereby uraninite is strikingly more abundant in the reddish and greenish envelopes than in the surrounding host granite.

Los Santos scheelite skarn deposit

Los Santos scheelite skarn is located along the contact between the granite and the Upper Vendian to Lower Cambrian metasedimentary rocks on the northern limb of the Tamames syncline (Fig. 1C). The skarn is made up of a series of meter-thick lenticular bodies of mineralized pyroxene skarn, which occur in a zone less than 1km-long. They display a very complex geometry that is controlled by northeast-southwest-trending faults and dikes. The scheelite skarn of Los Santos occurs in the massive limestone and dolostone beds of 50 and 200m–thick, respectively, Tamames Limestones Fm. and in the transition zone to the Tamames Sandstones Fm., which consists of dark fine-grained greywacke. The mineralized skarn includes prograde skarn and its retrograde alteration. The prograde exoskarn is made up of a thick, almost monomineralic mass of hedenbergite, accompanied by grossular and Mo-rich scheelite (Sch I). It is associated with granite facies C and D, which developed endoskarn with calcic plagioclase and clinopyroxene. The retrograde skarn has a complex paragenesis that has been divided into two substages (Timón *et al.*, 2009). The first substage is made of anorthite, zoisite, apatite, titanite, quartz, sulfides (mainly pyrrhotite linked to strong silicification and epidotization) and subcalcic garnet associated with the leaching of early scheelite and the precipitation of Mo-poor scheelite (Sch II). The second substage is characterized by the formation of clinozoisite, prehnite, quartz, calcite, chlorite, white mica, zeolite and mineral phases belonging to the Bi-Te-Ag-S-Au system (Fig. 2).

In Los Santos skarn zone, uraninite occurs in the aplitic fragments, as well as in Ca-metasomatic rocks. Uraninite is hosted by K-feldspar crystals in the prograde endoskarn and is included in calcic plagioclase and associated with mineral phases typical of the retrograde stage of the skarn development.

METHODS

Samples were collected from Los Santos and El Cabaco ore deposits. A Geiger counter was used to select samples for alpha-autoradiography using cellulose nitrate film (Fig. 3A) (Basham and Easternbrook, 1977; Basham, 1981). Each sample was initially studied in polished thin sections (Fig. 3B). The petrographic observations to identify uraninite and determine its mode of occurrence were carried out using a Leica DM RD polarized microscope. High-resolution backscattered electron images were generated to examine within-grain compositional heterogeneity.

Major, minor and trace element compositions of uraninite were determined using a JEOL Hyperprobe JXA-8500F with a thermal field-emission cathode at Deutsches GeoForschungs Zentrum (GFZ) in Potsdam, Germany. The following analytical conditions were used: 20kV acceleration voltage, 20nA beam current, 1–2μm beam diameter, and 20s peak counting times for Pb, U and Fe, 30s for Y and Si, 40s for Ca and Th, and 50s for the REEs. The CITZAD routine in the JEOL software, which is based on the Φ(ρZ) method (Armstrong, 1995), was used for data processing.

There are several methods for chemical age calculation on the basis of the chemical composition of uranium-rich minerals (Bowles, 1990). All these methods assume that all lead contained in the mineral, uraninite in this case, is radiogenic and that there was no mobility of lead, uranium and thorium. Single point ages were obtained using the iteration of the formula:

$$PbO = ThO_2 k_0 (\exp(\lambda_{232} t)-1) + UO_2 (k_1(\exp(\lambda_{238} t)-1) + k_2 (\exp(\lambda_{235} t)-1))$$

where t is the time in years, $\lambda_{232}=4.9475\times10^{-11}y^{-1}$, $\lambda_{235}=9.8485\times10^{-10}y^{-1}$ and $\lambda_{238}=1.55125\times10^{-10}y^{-1}$ are the decay constants of ^{232}Th, ^{235}U and ^{238}U, respectively (Steiger and Jäger, 1977). The constants $k_0=0.848485$, $k_1=0.816367$ and $k_2=0.0059475$ account for the molecular weight ratios and isotopic abundances. Reproducibility was tested by repeated measurements of the same spot (*e.g.* Finger *et al.*, 2017; Förster *et al.*, 2012).

For chemical dating of uraninite, initial incorporation of Pb is irrelevant in comparison with *in situ* Pb growth. For that reason, this approach makes it possible to date single uraninite crystals and to combine the chemical composition with the age of different parts of individual grains to characterize and possibly date the hydrothermal alteration (Pal and Rhede, 2013). Uraninite ages were calculated with ISOPLOT 3.0 software (Ludwig, 2003). The accuracy of the dating procedure was monitored using uraninite of known ID-TIMS age (*e.g.* Finger *et al.*, 2017). For age calculation we assigned an uncertainty of ±10Ma to each spot.

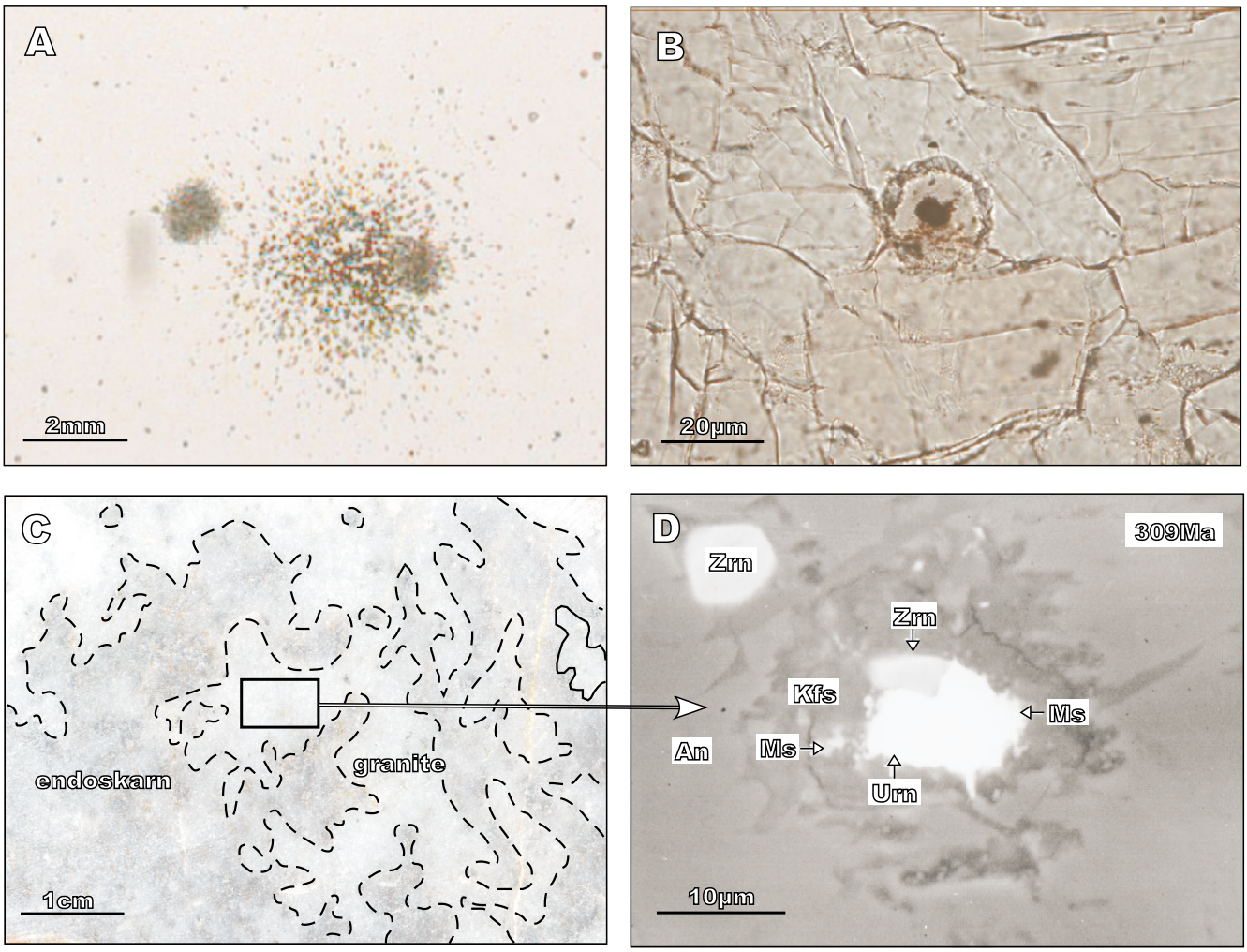

FIGURE 3. A) Autoradiography using Cellulose Nitrate (CN) film showing alpha track clusters of uraninite grains. B) Photomicrograph illustrating the metamict aureole of a Group-I uraninite. C) The endoskarn of Los Santos with relicts of aplite granite (sample S47-3). The dashed line delimits the aplite granite and the darker metasomatized zone (endoskarn). D) Backscattered electron image of Group-Ia Uraninite (Urn) hosted in a K-feldspar (Kfs) crystal. Zircon (Zrn), Anorthite (An) and aggregates of white Mica (Ms) can be observed.

URANINITE CHARACTERIZATION

Based on chemical, textural and morphological characteristics, which are directly related to mineral assemblages, two uraninite groups are differentiated: Group-I and Group-II in Los Santos skarn and Group-II in El Cabaco quartz veins. Characteristics of the two types of uraninite are described below. Their chemical composition is shown in Table 1 and in Figures 4 and 5.

Group-I uraninite

This type of uraninite only occurs as relics in some of the endoskarn samples (Fig. 3C, D). It forms octahedral inclusions in K-feldspar. Uraninite crystals are typically only 10 to 20µm-large and developed a radiation-damage aureole. The uraninite crystals show total oxide contents ranging between 89.75wt.% and 91.88wt.%, relatively low UO_2 (76.01–80.39wt.%), restricted PbO (3.23–3.34wt.%) and substantial ThO_2 contents (6.95–8.51wt.%) (Fig. 4A; Table 1). Group-I uraninite includes two groups with contrasting REEs concentrations. Group-Ia has $\sum REE_2O_3$ contents between 1.26 and 1.83wt.%, whereas Group-Ib has $\sum REE_2O_3$ contents between 0.55 and 0.67wt.% (Fig. 4B). Group-I uraninite has Ca and Si contents below detection limit and a low FeO content (average=0.31wt.%). The contents of UO_2 are slightly higher in Group-Ib, whereas those of ThO_2 are slightly higher in the Group-Ia type.

Group-II uraninite

Group-II uraninite differs from Group-I uraninite both in chemical composition and texture. The total oxide content of the Group-II uraninite varies between 88.72 and 95.15 (Table 1). Group-II uraninite have higher contents of UO_2 (84.29–89.54wt.%) (Fig. 4A, B) than Group-I

TABLE 1. Compositions and calculated ages of uraninite from Los Santos and El Cabaco ore deposits (oxides are in wt.%)

Sample	Nº	SiO_2	CaO	FeO	ThO_2	UO_2	PbO	La_2O_3	Ce_2O_3	Nd_2O_3	Y_2O_3	Sm_2O_3	Gd_2O_3	Tb_2O_3	Dy_2O_3	Er_2O_3	Yb_2O_3	Ho_2O_3	Pr_2O_3	Lu_2O_3	Total	$\sum REE_2O_3$	Age(Ma)
GROUP-Ia uraninite hosted by K-feldspar in the aplitic fragments (Los Santos)																							
S47-3-Ed	42	b.d.l.	b.d.l.	0.38	8.35	76.26	3.33	0.02	0.01	0.04	0.43	n.d	0.32	0.09	0.21	0.08	0.13	0.12	n.d	n.d	89.77	1.45	309
S47-3-Ed	45	b.d.l.	b.d.l.	0.20	8.26	76.78	3.26	n.d	0.03	0.08	0.42	n.d	0.20	n.d	0.19	0.13	0.10	0.01	0.11	n.d	89.76	1.26	301
S47-3-Ed	46	b.d.l.	b.d.l.	0.17	8.51	76.01	3.23	0.08	n.d	0.20	0.83	0.06	0.15	n.d	0.07	0.14	0.13	n.d	0.09	0.09	89.75	1.83	301
S47-3-Ed	47	b.d.l.	b.d.l.	0.30	7.85	77.91	3.26	0.04	0.05	0.13	0.44	n.d	0.04	0.04	0.14	0.20	0.10	0.01	0.10	n.d	90.60	1.27	298
GROUP-Ib uraninite hosted by K-feldspar in the aplitic fragments (Los Santos)																							
S47-3-Eb	44	b.d.l.	b.d.l.	0.34	7.16	79.58	3.32	0.05	n.d	0.07	n.d	n.d	0.08	0.12	0.05	0.06	n.d	0.04	0.03	0.05	90.96	0.55	298
S47-1-8	74	b.d.l.	b.d.l.	0.41	6.95	80.39	3.34	0.08	n.d	0.22	0.08	0.04	0.05	0.06	0.04	0.05	0.06	n.d	n.d	n.d	91.88	0.67	297
Average age of Group-I uraninite from Los Santos: 300±4																							
GROUP-II uraninite hosted by anorthite and minor K-feldspar (Los Santos)																							
S47-3-C	36	n.d	n.d	0.03	0.86	86.47	3.48	0.11	0.03	n.d	0.02	0.12	0.03	0.09	n.d	0,07	n.d	n.d	n.d	0.04	91.35	0.51	294
S47-3-C	37	n.d	n.d	0.12	0.66	84.34	3.37	n.d	0.01	0.08	n.d	n.d	n.d	n.d	n.d	n.d	0.03	0.08	n.d	0.03	88.72	0.22	292
S47-1-5	64	n.d	n.d	0.04	1.03	89.54	3.69	0.06	0.04	0.02	0.05	0.06	0.01	0.02	0.13	0.07	0.02	n.d	n.d	0.02	94.83	0.50	301
S47-1-5	65	n.d	n.d	0.08	0.54	89.47	3.58	n.d	n.d	n.d	0.08	0.11	n.d	0.08	0.04	0.05	n.d	0.02	n.d	n.d	94.06	0.38	293
S47-1-5	66	n.d	n.d	0.05	0.67	89.21	3.58	n.d	0.06	0.02	n.d	0.04	0.19	0.01	0.09	n.d	0.02	0.05	n.d	0.08	94.03	0.52	294
S47-1-6	68	n.d	n.d	0.12	1.60	88.67	3.68	n.d	0.03	0.01	0.08	n.d	0.02	n.d	0.02	0.02	0.04	n.d	0.07	n.d	94.36	0.29	302
S47-1-7C3	69	n.d	n.d	0.25	0.57	88.91	3.63	0.03	0.02	0.02	n.d	0.18	0.09	0.06	n.d	0.08	0.03	0.07	0.06	n.d	94.00	0.63	299
S47-1-7C3	70	n.d	n.d	0.28	1.87	88.09	3.63	0.10	0.10	n.d	n.d	0.01	n.d	0.05	0.12	0.04	n.d	0.07	n.d	n.d	94.36	0.49	300
S47-1-7C3	71	n.d	n.d	0.26	0.90	88.44	3.65	n.d	n.d	0.12	n.d	n.d	n.d	n.d	n.d	0.12	n.d	0.18	0.05	n.d	93.72	0.46	301
S47-1-9	72	n.d	n.d	0.90	1.47	87.72	3.58	0.02	0.04	0.07	n.d	0.09	0.13	n.d	n.d	n.d	0.02	0.03	0.07	0.05	94.19	0.51	298
GROUP-II uraninite hosted by albite (El Cabaco)																							
2138B-4	25	n.d.	n.d	0.64	0.82	88.95	3.56	0.02	0.05	0.06	0.09	0.05	0.12	n.d	0.13	n.d	0.02	0.04	n.d	0.02	94.57	0.60	293
2138B-4	26	0.02	n.d	0.59	0.85	88.66	3.57	0.14	n.d	n.d	0.17	n.d	n.d	0.16	n.d	0.09	0.02	0.08	0.05	n.d	94.39	0.70	294
2138B-4	27	n.d.	n.d	0.70	0.78	89.38	3.64	n.d	n.d	0.04	0.11	0.13	0.10	0.04	0.01	0.12	n.d	0.05	0.03	0.02	95.15	0.65	298
2138B-5	28	n.d.	n.d	0.33	1.41	87.04	3.59	n.d	0.06	n.d	0.15	0.07	0.09	n.d	0.13	0.05	0.01	n.d	0.11	0.05	93.09	0.72	301
2138B-5	29	n.d.	n.d	0.27	1.45	86.79	3.49	n.d	n.d	n.d	0.20	0.04	0.13	n.d	n.d	n.d	0.06	n.d	0.01	n.d	92.44	0.44	293
2138B-5	30	n.d.	n.d	0.18	1.40	87.49	3.48	0.02	n.d	n.d	0.20	0.11	0.14	0.04	0.11	n.d	0.06	n.d	0.06	0.03	93.32	0.77	290
44A-1	48	n.d.	n.d	0.39	0.41	89.43	3.57	0.10	0.01	n.d	0.10	n.d	0.12	n.d	0.14	n.d	0.08	n.d	0.01	n.d	94.37	0.57	292
44A-1	49	n.d.	n.d	0.30	0.53	89.03	3.63	0.03	n.d	n.d	0.08	n.d	0.04	0.06	0.16	n.d	0.09	0.05	0.04	0.05	94.09	0.60	298
44A-1	50	n.d.	n.d	0.18	0.57	88.84	3.54	0.05	0.05	n.d	0.09	0.06	0.10	n.d	n.d	0.04	n.d	0.12	n.d	0.01	93.66	0.53	292
2138AF2-1	51	n.d.	n.d	0.23	1.67	86.73	3.48	0.05	n.d	0.02	0.15	n.d	0.07	0.03	0.14	0.07	0.06	n.d	n.d	0.02	92.72	0.61	292
2138AF2-1	52	0.04	n.d	0.16	1.88	85.90	3.44	n.d	n.d	0.05	0.20	0.01	0.07	n.d	0.06	0.05	0.01	0.09	0.21	0.05	92.23	0.82	292
2138AF2-2	54	0.06	n.d	n.d	1.37	86.96	3.47	0.03	0.01	0.03	0.12	0.02	0.24	0.05	n.d	0.13	0.02	0.06	n.d	0.02	92.60	0.74	291
Average age of Group-II uraninite associated with plagioclase from both deposits: 296±2																							
GROUP-II uraninite associated with sulfides and tungsten (Los Santos)																							
S47-3-B	34	n.d.	n.d.	0.25	0.93	88.64	3.52	n.d	0.02	0.12	0.13	n.d	0.09	n.d	0.16	n.d	0.05	n.d	n.d	n.d	93.91	0.57	290
S47-3-B	35	n.d.	n.d.	0.23	0.98	87.99	3.49	n.d	n.d	n.d	0.08	n.d	0.05	0.06	n.d	n.d	0.11	n.d	n.d	n.d	92.99	0.30	290
S47-3-Eb	43	n.d.	n.d.	0.23	3.61	84.29	3.33	n.d	n.d	0.03	n.d	0.02	n.d	n.d	0.06	0.07	n.d	n.d	0.02	0.01	91.67	0.21	286
GROUP-II uraninite associated with sulfides and tungsten (El Cabaco)																							
2138A-A	59	n.d.	n.d.	0.66	0.63	88.59	3.48	n.d	n.d	0.07	0.22	0.15	0.09	0.11	0.02	n.d	0.06	0.19	n.d	0.01	94.30	0.90	288
2138A-A	60	0.03	n.d.	0.74	1.00	88.05	3.40	n.d	n.d	0.04	0.32	0.13	0.19	0.02	0.11	0.10	0.04	n.d	n.d	n.d	94.16	0.94	282
Average age of Group-II uraninite associated with sulfides and tungsten from both deposits: 287±4																							

Notes: n.d.: not detected.

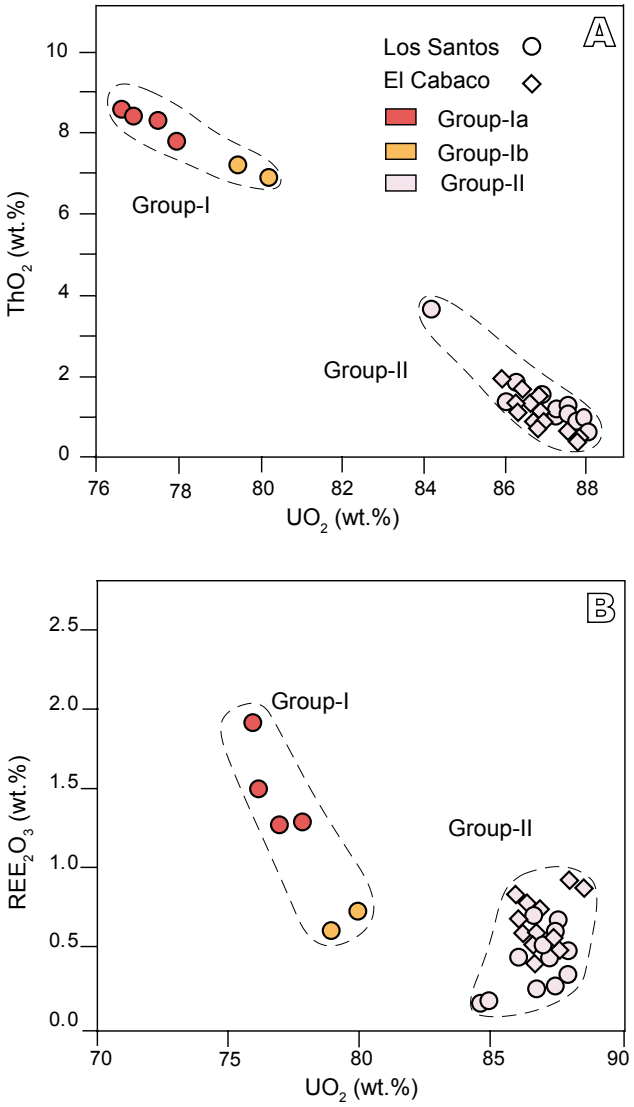

FIGURE 4. Concentrations (in wt.%) of different major and minor elements in uraninite. A. UO_2 *vs.* ThO_2 plot shows that Group-I uraninite is characterized by a higher content in ThO_2 than Group-II uraninite. B. REE_2O_3 contents of Group-I uraninite divide Group-I into two subgroups, -Ia and -Ib.

uraninite and lower contents of ThO_2 (0.41–3.61wt.% and $\sum REE_2O_3$ (0.94–0.21wt.%) (Fig. 4A, B). Ca and Si contents are near or below detection limit (Table 1) and the FeO content is low (average=0.31wt.%); its relationship with $\sum REE_2O_3$ and UO_2 is shown in Figure 5A, B.

In Los Santos district, Group-II uraninite forms small (10–15µm) round grains and occurs in the high temperature endoskarn, next to relicts of aplite granite (Fig. 6A), which was affected by K-feldspar alteration. Group-II uraninite grains from the endoskarn are included K-feldspar crystals and the uraninite radiation-damage aureole often contains U-rich micas and Fe-oxide-hydroxides (Fig. 6B, C). Group-II uraninite also occurs in the anorthite skarn, the retrograde alteration of Los Santos endoskarn (Fig. 6D). In the anorthite skarn, this uraninite is included in anorthite crystals, which are altered to epidote group minerals (Fig. 6E, F). In the metamict aureoles of the uraninite from the anorthite skarn, K-feldspar is missing. In Los Santos deposit, a large uraninite grain included in K-feldspar crystals, without sulfides in the mineral association, displays two compositional zones (Fig. 7). The compositional variation observed within single uraninite grains is indistinguishable from the groups defined on the deposit scale.

In El Cabaco ore deposit, Group-II uraninite occurs predominantly in reddish and greenish halos surrounding quartz veins (Fig. 8A-C) and more rarely in altered granite. Uraninite of this district can be hosted by plagioclase, white mica or quartz, and individual uraninite crystals may reach up to 120µm (Fig. 8B).

In both districts, Group-II uraninite also occurs in silicified zones typically associated with sulfides and scheelite (Figs. 6, 8) and the composition of these uraninite grains is similar to that of the rest of Group-II, except for the lower PbO (3.33–3.52wt.%) contents, which reflect the younger age of this uraninite.

CHEMICAL DATING OF URANINITE

Electron probe dating of uraninite shows age variations from 282 to 309Ma (Table 1). Group-I uraninite yields chemical ages in the range of 297–309Ma. The average age of Group-I uraninite is 300±4Ma. The oldest age of 309Ma is obtained from a Group-Ia uraninite included in a K-feldspar crystal in the leucogranite. Group-II uraninite yields generally younger chemical ages that range from 282 to 302Ma (Table 1) with some overlap with Group-I uraninite. Differentiating Group-II uraninite according to mineral paragenesis and textural relations indicated that there may be two younger groups of uraninite with average ages of 296±2Ma, specifically uraninite in association with anorthite in Los Santos Skarn and secondary albite in El Cabaco, and 287±4Ma for uraninite associated with the silicification event with sulfides and tungsten in both deposits (Fig. 5C).

Chemical ages also vary within individual uraninite grains (Fig. 7). Zone A, with Group-I composition, yields a chemical age of 298Ma, and Zone B, with Group-II composition, yields a chemical age of 286Ma. The older age is obtained for a compositionally homogeneous zone that shows octahedral crystal habit, whereas the younger age is recorded in a zone where uraninite crystals are anhedral to subhedral.

DISCUSSION

Compositional variations in uraninite

Uraninite, UO_2, may contain considerable amounts of ThO_2 (up to 11wt.%), REEs (up to 4wt.% ∑REE), Y (up to 1.3wt.%), and depending on age- radiogenic lead (Finch and Murakami, 1999; Förster, 1999; Frimmel *et al.*, 2014; Janeczek and Ewing, 1992). Uraninite is a chemically active mineral and may change its composition as it recrystallizes during interaction with fluids (Alexandre and Kyser, 2005; Finch and Ewing, 1992; Kempe, 2003; Pal and Rhede, 2013). The two uraninite-types differentiated in this work could represent two different events of uranium mineralization or successive modifications of pristine uraninite by superimposed hydrothermal processes. It is commonly accepted that thorium and REEs are not mobile in fluids (Keppler and Wiley, 1990) and high contents in Th and REEs have been documented from magmatic uraninite [ThO_2 ranging from 5.6 to 11wt.% in biotite granites (see Förster, 1999); REEs between 0.05 and 4wt.% (see Frimmel *et al.*, 2014)]. Therefore, Group-I uraninite from Los Santos, with contents in thorium between 7 and 8.5wt.% and REEs ranging between 0.6 and 1.8wt.%, exhibits values of magmatic uraninite and may represent primary uraninite related to the magmatic system rather than hydrothermal uraninite. Other chemical features, such as the absence of CaO and SiO_2, which points to the lack of coffininite or various uranyl silicates typical of alteration (Frimmel *et al.*, 2014) and a U/Th ratio *ca.* 10 (magmatic uraninites have values <200, see Frimmel *et al.*, 2014), also seem to be typical for uraninite that formed from granitic residual fluids (Hazen *et al.*, 2009; Plant *et al.*, 1999). Additionally, Kempe (2003) interpreted the association of uraninite with zircon, similar to that of Group-I uraninite and zircon in Figure 3D, as a magmatic feature, which also supports the magmatic character of the Group-I uraninite. Moreover, Group-Ib uraninite has slightly lower Th, Y and REEs contents than Group-Ia. Group-Ib uraninite could represent a late uraninite in relation to K-feldspar alteration, a modification of the pristine uraninite by fluids related to feldspatization, or a magmatic uraninite that is depleted in Th, Y and REEs because of the strong fractionation of these elements by Group-Ia uraninite or monazite. A magmatic formation of uraninite seems probable for two reasons: i) REEs and ThO_2 contents are in the range of magmatic uraninites; and ii) recrystallization of magmatic uraninite would release Th, Y and REEs, which are little mobile in fluids and, thus, should be sequestered in Th-Y-REEs-rich minerals close to the depleted uraninite. In contrast, Group-Ib uraninite is rimmed by Group-II uraninite, *i.e.* anhedral to subhedral Th-Y-REEs-poor uraninite (Fig. 7), which is not compatible with fluid interaction.

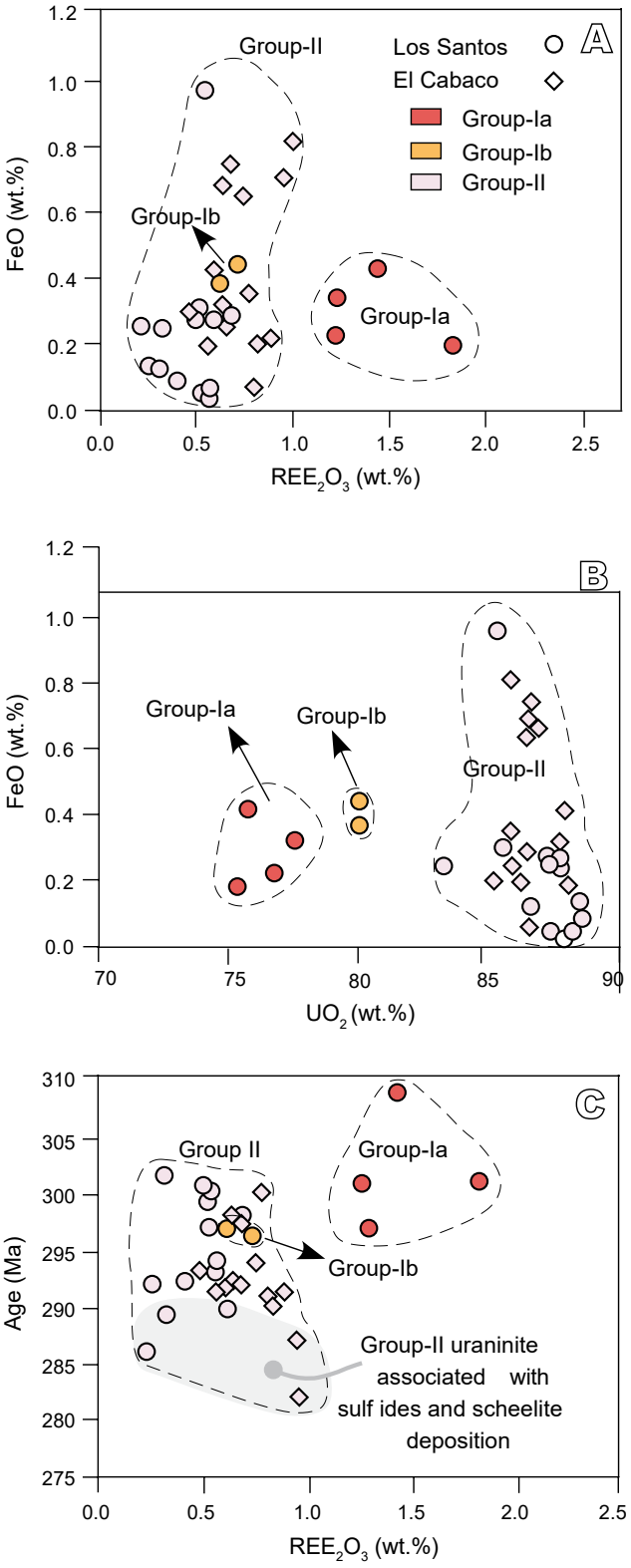

FIGURE 5. A–B)FeO *vs.* REE_2O_3 and UO_2 plots allow to distinguish Group-Ia uraninite from the other groups. C) Group-Ia, Group-II display different age ranges in age *vs.* REE_2O_3 plot. Group-Ib shows similar values as Group-II uraninite. Grey zone corresponds to uraninite from samples enriched in silica.

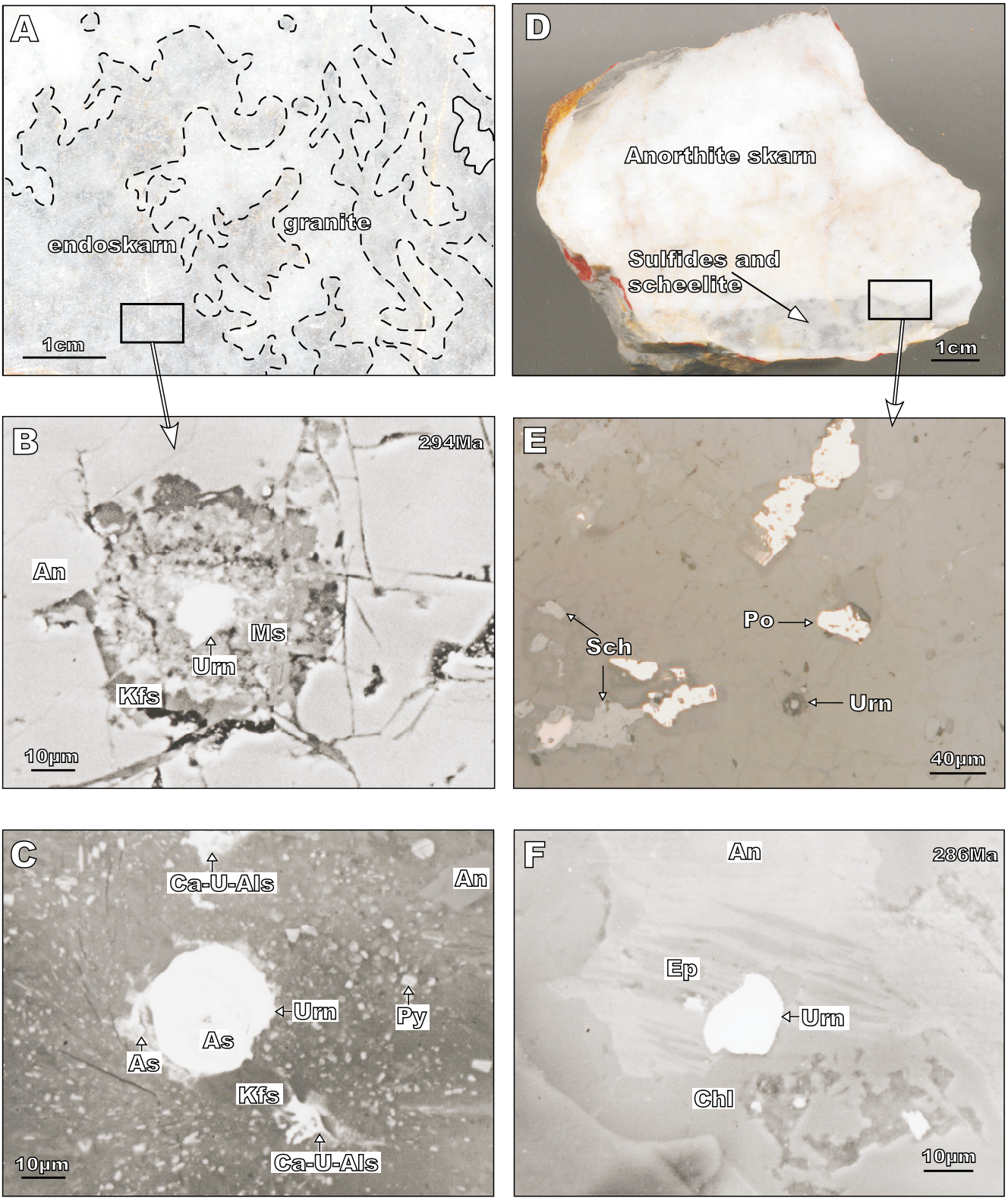

FIGURE 6. Group-II uraninites from the Los Santos skarn. A) Hand specimen of endoskarn with sections with Group-II uraninite. B) Backscattered electron image of Group-II Uraninite (Urn) included in K-feldspar (Kfs) crystal partly replaced by U-rich Muscovite (Ms) and surrounded by Anorthite (An). C) Backscattered electron image of disseminated Pyrite (Py), Ca- and U-Aluminosilicates (Ca-U-Als), K-feldspar (Kfs) and Anorthite (An) crystals in the radiation damage aureole of Group-II Uraninite (Urn). D) Anorthite skarn with sulfides and scheelite. E) Photomicrograph of Group-II Uraninite (Urn), Pyrrhotite (Po) and Scheelite (Sch). F) Backscattered electron image of Uraninite (Urn) grain occurring in Anorthite (An) groundmass accompanied by Epidote group minerals (Ep) and Chlorite (Chl).

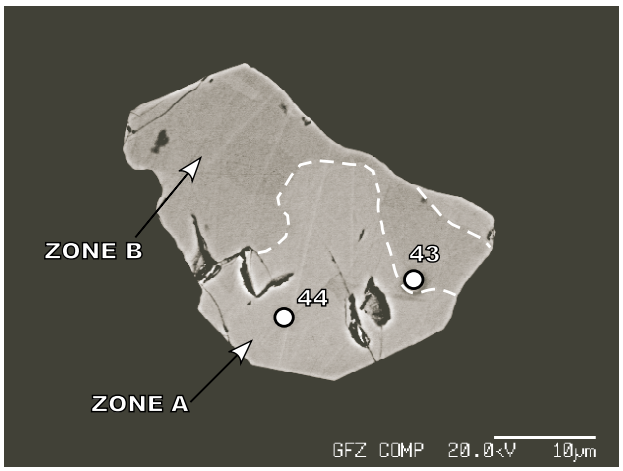

FIGURE 7. Backscattered electron image of a large uraninite grain showing two distinct zones. The brighter area (zone A) has higher ThO_2 (7.16wt.%) and $\sum REE_2O_3$ (0.55wt.%) contents than the darker area (zone B) 3.61wt.% ThO_2 and 0.21wt.% $\sum REE_2O_3$. Zone B appears surrounding the octahedral crystals of zone A. The composition of zone A uraninite resemble Group-Ib uraninite, whereas zone B uraninite is similar to Group-II uraninite. Numbers correspond to analysis numbers and to the calculated ages on individual spots given in Table 1.

Group-II uraninite from Los Santos skarn exhibits significantly lower Th and REEs contents than pristine Group-I uraninite. The low mobility of these elements in fluids suggests that Group-II uraninite is related to skarn formation. The low analytical totals of pristine uraninite probably reflect the presence of structural H_2O or hydroxyl groups (Alexandre and Kyser, 2005) or the higher oxidation state of elements present (Zachariáš *et al.*, 2008).

In El Cabaco deposit, no Th-REEs-enriched uraninite was found, and all crystals exhibit chemical features typical of Group-II uraninite of Los Santos skarn. Uraninite from El Cabaco deposit and Los Santos skarn shows the same age groups, even though ages are related to different locations and very different deposit types. This cluster of ages indicates that element redistribution occurred during distinct hydrothermal events related to large-scale tectonic processes, possibly operating at the scale of the Variscan orogen.

The alteration type in uraninite is a function, among other factors, of the chemical and physical characteristics of the available fluids, which in turn are related to host-rock lithology and structure. Of primary importance is the availability of elements in the fluid. Group-II uraninite shows Ca concentrations below detection limit. The low Si and Ca contents of uraninite in skarn may reflect the crystallization of calcium silicate minerals, such as epidote and anorthite, which acted as Si and Ca sinks, impoverishing the mineralizing solution and, thus, the uraninite in these elements.

Another factor to take into account is the redox state of the fluids. Uranium silicates tend to form under reducing conditions, whereas uranyl minerals form under oxidizing conditions (Finch and Murakami, 1999). Although later fluids in Los Santos scheelite skarn are oxidizing, the gradual interaction of magmatic fluids with the graphitic rocks of the Schist-Greywacke Complex resulted in a reduction in ore fluids (Timón *et al.*, 2009) and enhanced formation of uranium silicates such as the crystals that appear in the radiation damage of Group-II uraninite (see Fig. 6B). Thus, the chemical composition of uraninite is partly controlled by the composition of the host-rocks that may affect the redox state of the fluids.

The significance of the chemical uraninite ages from Los Santos and El Cabaco in the context of the Spanish Central System Batholith

Taking into account the compositional and textural features shown above, it may be inferred that the ages between 309 and 297Ma (average=300±4Ma) calculated for Group-I uraninite display the age of magmatic uraninite crystallization. This age overlaps with zircon ages (309 to 303Ma) from granites surrounding Los Santos skarn (Bea *et al.*, 2004; Díaz Alvarado *et al.*, 2013; Gutiérrez-Alonso *et al.*, 2011; Valle Aguado *et al.*, 2005; Zeck *et al.*, 2007).

The ages of hydrothermal Group-II uraninite (296±2 for K-alteration and 287±4Ma for assemblages with associated sulfides and tungsten) at Los Santos and El Cabaco may be placed within a broader scenario. Geochronological constraints of hydrothermal episodes in the western sector of the SCSB are scarce and not accurate, but several hydrothermal episodes related to the waning Variscan orogeny have been recognized in the eastern sector of the SCSB (Caballero *et al.*, 1992; Galindo *et al.*, 1994; Martín-Crespo *et al.*, 2004; Tornos *et al.*, 2000). These include W-Sn sulfides veins and greisens, Sn-W skarns, episyenites, scheelite sulfides-rich veins and greisens and barren quartz veins.

The oldest ages of the hydrothermal uraninite (*ca.* 296Ma could be related to the development of the prograde skarn at Los Santos and the oxide stage at El Cabaco (Fig. 9). In both districts, uraninite yielding this age is associated with new alkali and early tungsten deposition. The earliest metasomatic alteration coincides in time with the first episode of hydrothermal activity recognized in the eastern SCSB during the Upper Carboniferous, *ca.* 295Ma (Tornos *et al.*, 2000). The older hydrothermal rocks are restricted to minor skarns, as is the case of Sn-W Carro del Diablo skarn, formed by the replacement of marbles near the contact with a *ca.* 302Ma biotite granite stock (Casquet and Tornos, 1984). Another group of hydrothermal rocks is represented by

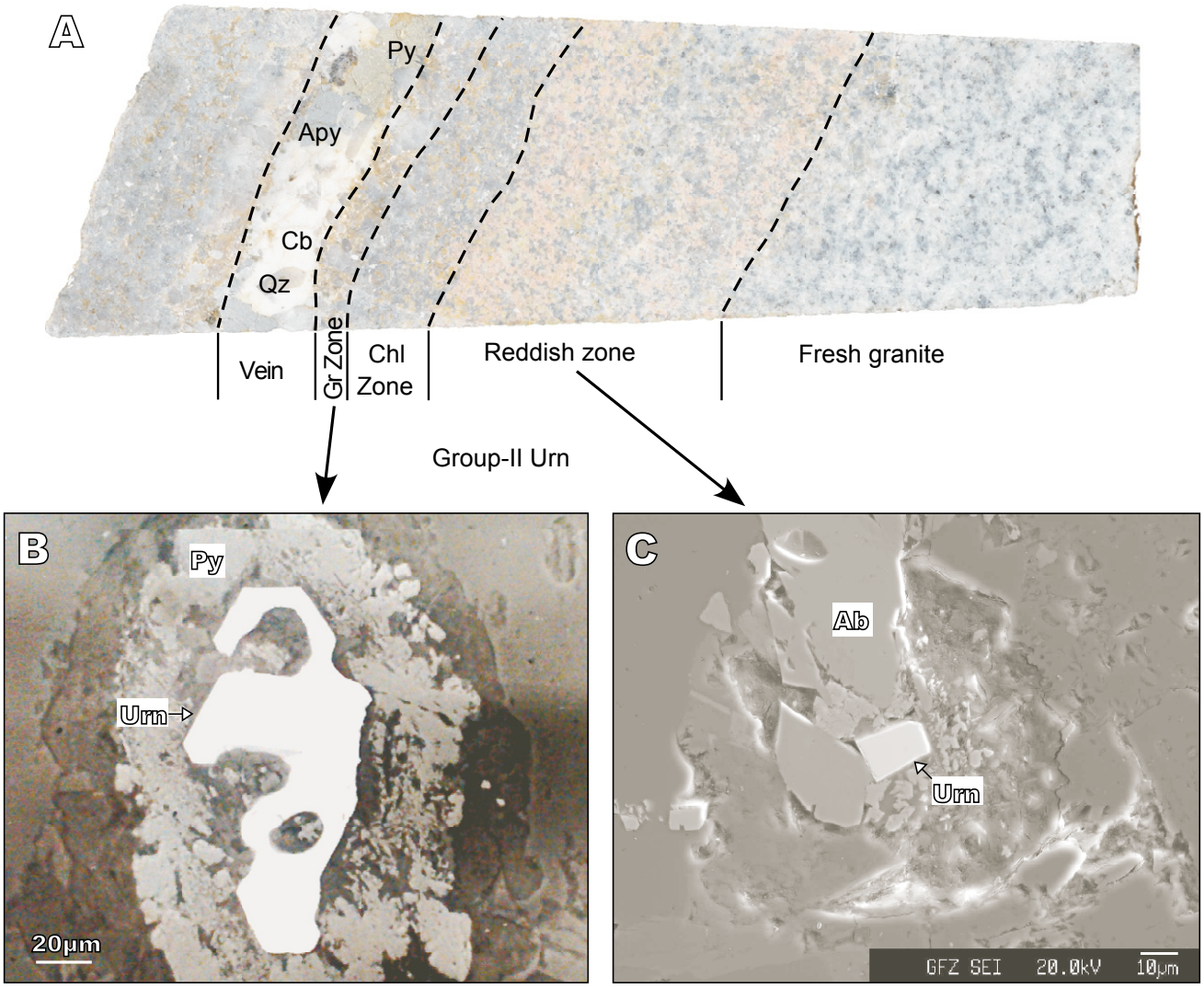

FIGURE 8. A) Hand specimen taken from the El Cabaco SA-8-1 drill-hole illustrating a mineralized quartz-vein, healed by Quartz (Qz), Arsenopyrite (Apy), Pyrite (Py) and Carbonates (Cb), hosted by inequigranular biotite granite. The vein mineralization includes As-Fe sulfides, scheelite and uraninite. From the contact with the vein to the fresh granite, there is a selvage-style Greisen (Gr Zone), a Chlorite-rich zone (Chl Zone) and the granite transformed into episyenite (Reddish Zone). B) Backscattered electron image of a Group-II Uraninite (Urn) associated with Pyrite (Py). C) Backscattered electron image of Group-II Urn hosted by Albite (Ab).

the W-(Sn)-bearing quartz veins and fracture-controlled greisens (Vindel *et al.*, 1995) that have provided K-Ar ages between 302±6 and 291±8Ma (Caballero *et al.*, 1992). Hydrothermal muscovites coeval with sulfides, using the $^{40}Ar/^{39}Ar$ method at As-(Ag) sulfide veins at Mónica Mine (Bustarviejo) provided 286±4Ma for this mineralizing event (Martín-Crespo *et al.*, 2004). These rocks are commonly found in relation to apical zones of leucogranites (Tornos *et al.*, 1993) and they formed during strike-slip faulting after the Variscan orogeny (González Casado *et al.*, 1996).

Uraninites yielding a younger age (close to 287Ma) are associated with the greenish muscovite-enriched selvage of quartz veins of El Cabaco and the mineral association typical of the retrograde skarn at Los Santos (Fig. 9). They are associated with the precipitation of late scheelite linked to the main sulfides deposition and silicification process. A widespread precipitation of scheelite, arsenopyrite and metal base sulfides developed during the reactivation of W-quartz vein which occurred during the second hydrothermal event identified in the eastern part of the SCSB. A Permian age of this event (267±7Ma) was determined from K-Ar on muscovite (Tornos *et al.*, 1993). Probably synchronously, another group of hydrothermal metasomatic rocks represented by barren episyenites developed *ca.* 277Ma in the SCSB (Rb-Sr internal isochron ages; Caballero *et al.*, 1996, 1993), an age that is like that reported in gold- and uraninite-bearing episyenites close to the SCSB (270±12Ma,

López-Moro *et al.*, 2013). A similar age has also been reported for a subsolidus overprint recorded in allanite of vaugnerite rocks from the Tormes dome (275Ma, U-Pb ID-TIMS; López-Moro *et al.*, 2017). $^{40}Ar/^{39}Ar$ dating of muscovites of the granite- and gneiss-hosted barren quartz veins at the Guadarrama sector in the SCSB has provided ages of 274±5Ma (Martín-Crespo et al., 2002). Thus, the younger ages yielded by uraninite associated with abundant sulfide and silica deposition in Los Santos and El Cabaco districts could correspond to a second hydrothermal event recognized on a regional scale.

The last stage of mineralization, *i.e.* the gold stage, does not have associated uraninite (Fig. 2; González-Sánchez, 2003; Timón *et al.*, 2009). Therefore, its age is not known. A maximum age is given by the *ca.* 287Ma old sulfides stage. Gold mineralization, however, may be distinctly younger, as indicated by K-Ar muscovite ages, which range in the eastern SCS between 265±4 and 216±4Ma (Caballero *et al.*, 1992). This younger reactivation may also account for the resetting of K-Ar muscovite ages from salbands of El Cabaco mineralized veins (255–256±5Ma; Antona, 1991), 30Ma younger than the U-Pb chemical ages of uraninite. (Fig. 9).

Late-Variscan hydrothermal mineralization

Paleozoic tin-tungsten mineralization in Central and Western Europe and Atlantic North America define a discontinuous belt of several thousand kilometers in length. Mineral deposits within this belt are related to the Variscan-Appalachian orogenic belt, which was formed by the closure of the Rheic Ocean during the collision of Gondwana with Laurussia and the final assemblage of Pangea, and define three age groups, *i.e.* 400–360Ma, 335–310Ma, and 300–275Ma (Romer and Kroner, 2016 and reference therein). Mineralization of the 300–275Ma age group is related to a reorganization of the plate movement between Gondwana and Laurussia,

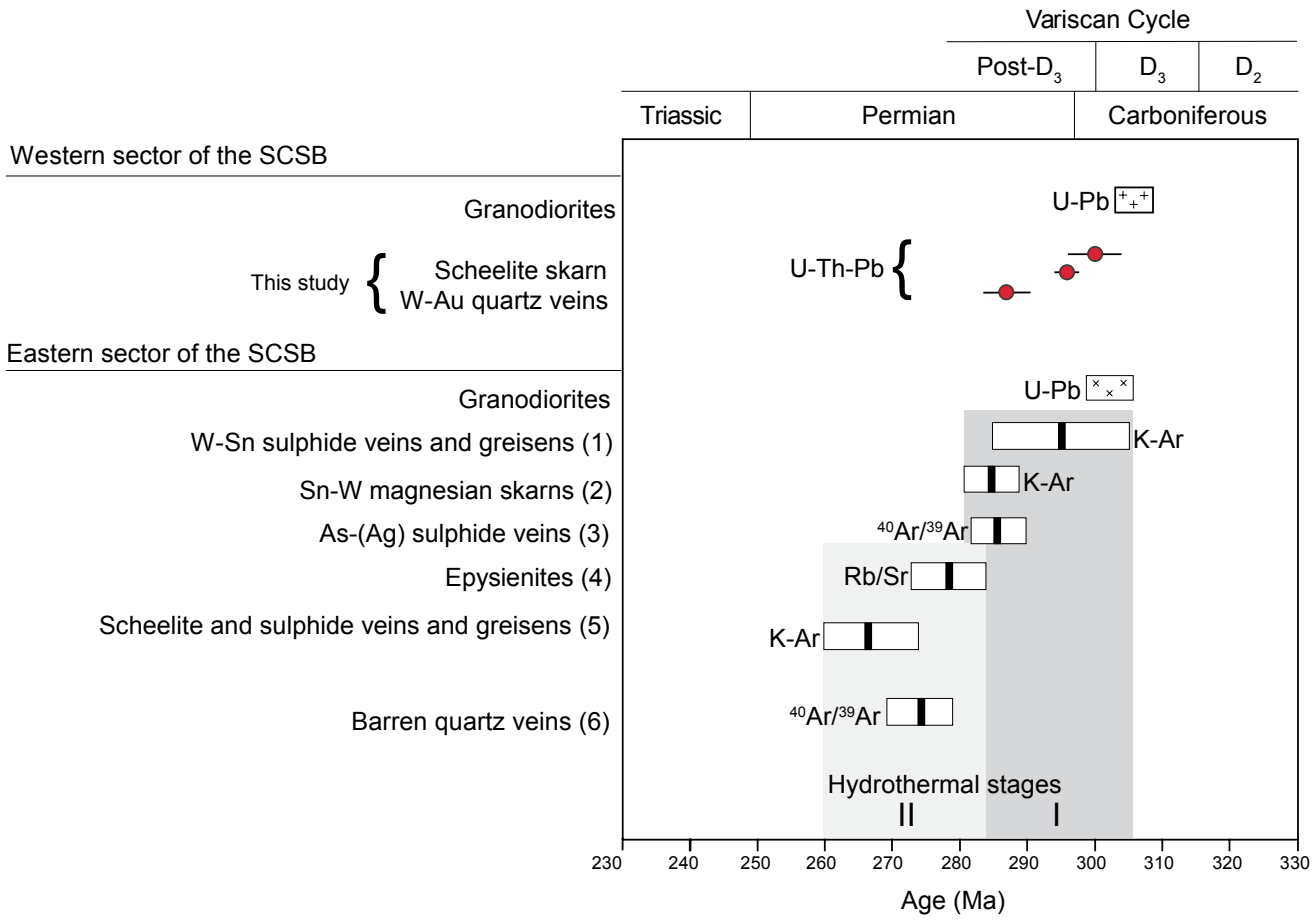

FIGURE 9. Diagram showing the age relationships of hydrothermal processes, intrusions and tectonic evolution in the Spanish Central System Batholith. Chemical uraninite ages and their error ranges (300±4, 296±2 and 287±4Ma) are included. Ages of hydrothermal events in the eastern SCSB are from data of Vindel *et al.* (1995) and Tornos *et al.* (2000) (1) (2) (4) (5); Martín-Crespo *et al.* (2004) (3); and Martín-Crespo *et al.* (2002) (6). The ages of granodiorites are from Orejana *et al.* (2012) and Díaz Alvarado *et al.* (2013). All Rb-Sr ages were recalculated using the decay constant recommended by IUGS (Villa *et al.*, 2015).

which resulted in widespread extensional tectonics in Central Europe (Chen *et al.*, 1993; Cuney *et al.*, 2002; Marignac and Cuney, 1999; Romer *et al.*, 2010). Crustal extension was associated with localized heat input from the mantle that accounts for Sn and W mineralization in the Variscan foreland, *i.e.* Cornwall and Slovakia, and locally also in the internal parts of the Variscan orogeny, *i.e.* the Saxo-Thuringian Zone, the French Massif Central and NW Iberia (Fig. 10). However, in internal parts of the Variscan orogen, there is also an older (325–318Ma), significantly more important, generation of Sn and W mineralization that is related to granitic magmatism after the continental collision (Förster *et al.*, 1999; Romer *et al.*, 2007).

For high-temperature Sn and W mineralization of Central and Western Europe, isotopic dating shows close correspondence between the age of granite emplacement and mineralization (Chesley *et al.*, 1993; Chicharro *et al.*, 2016; Darbyshire and Sheperd, 1985; Romer *et al.*, 2007). There is, however, increasing evidence of important hydrothermal mineralization that shows spatial closeness to igneous rocks, but which is much younger than the igneous activity. The spatial distribution of these hydrothermal mineralizations may indicate that the igneous rocks were involved as metal sources for these younger mineralizations or affected the distribution of the structures reactivated during younger tectonic processes. These younger hydrothermal mineralizations are structurally controlled. As these regionally widely separated mineralizations show a similar age distribution that closely corresponds to changes in the regional stress pattern affecting Central and Western Europe, they may have been controlled by the same overall process. For

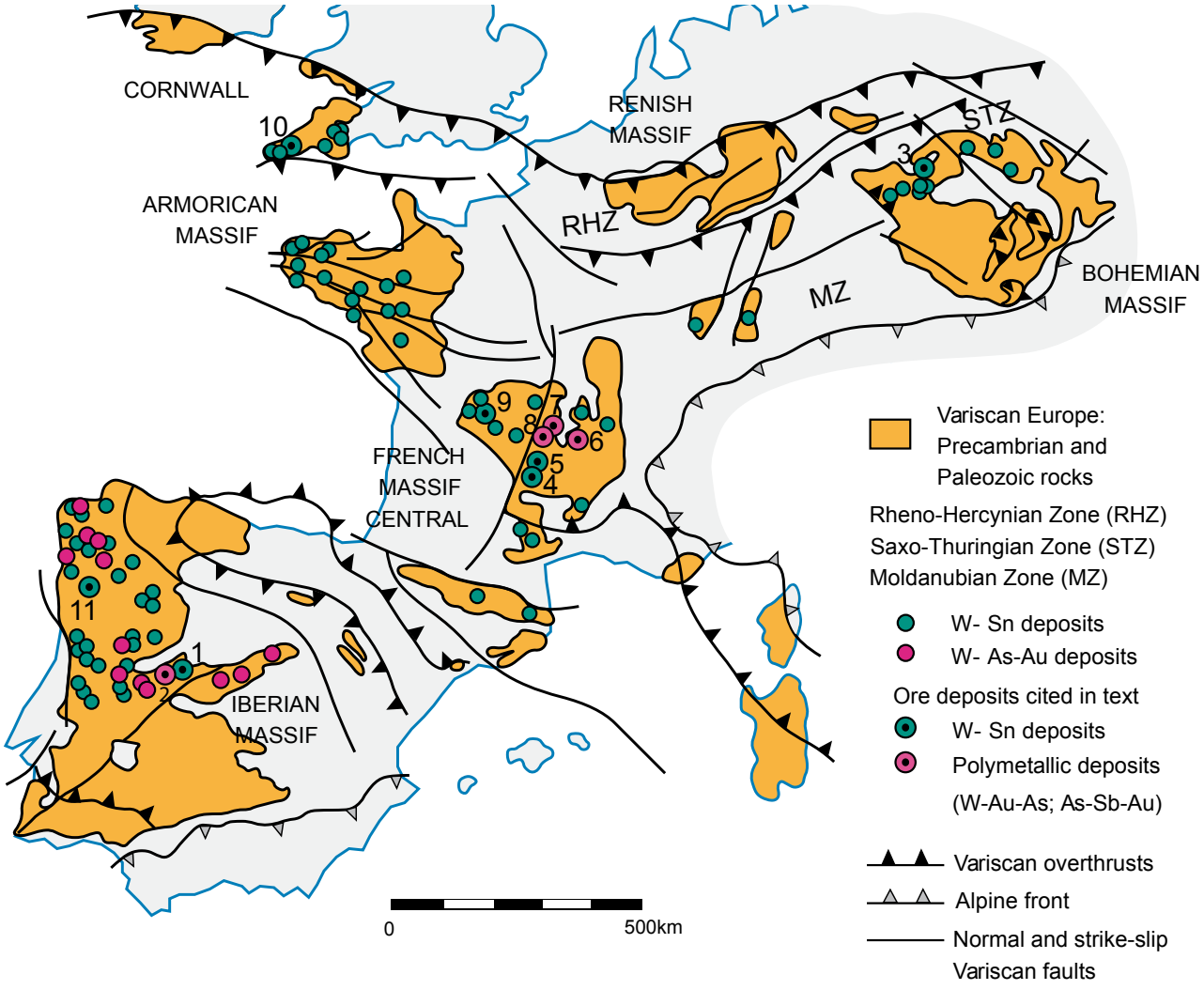

FIGURE 10. Map of the Variscan belt in central and western Europe (modified from Díez-Montes, 2007) and major W-Sn and some polymetallic deposits. Numbers correspond to the ore deposits mentioned in this study: Iberian Massif (1: Los Santos; 2: El Cabaco; 11: Carris), Bohemian Massif (3: Gottesberg), French Massif Central (4: Enguialès; 5: Leucamp; 6: Brioude-Massiac; 7: Pointgibaud; 8: Labessette; 9 Vaulry), southwest England (10: Cornwall).

instance, the *ca*. 300–275Ma old mineralization, formed when Central and Western Europe experienced crustal extension as result of the changing movement between Gondwana and Laurussia to close the remmants of the Rheic Ocean between North America and Africa (*e.g.* Kroner *et al.*, 2016). Even younger reactivations of the same structural elements, in some regions with related mineralization, occurred during the opening of the Tethys and the North Atlantic (Cathelineau *et al.*, 2012; Romer *et al.*, 2010).

Examples for late-Variscan mineralization in the Saxo-Thuringian Zone include 300–290Ma old Sn-W greisen at Gottesberg, which shows a time gap of at least 20Ma with respect to the Eibenstock granite intrusion (Kempe *et al.*, 2004) and in particular Permian fault-bound U mineralization that became redistributed during later tectonic events (*e.g.* Förster and Haak, 1995; Romer *et al.*, 2010), as well as Triassic and younger Ba-F veins. Late-Variscan mineralization in the French Massif Central include tungsten mineralization from the Vaulry, Leucamp and Enguialès deposits (298–274Ma) (Harlaux *et al.*, 2018) and polymetallic mineralizations such as W-Au-As and As-Sb-(Au) veins of Brioude-Massiac, Pb-Ag and As-Sn veins of Pontgibaud, and As-Pb-Sb-Au veins of Labessette (Bril *et al.*, 1991; Marignac and Cuney, 1999). In Cornwall, high-temperature Sn-W mineralization related to granite yields ages of 293.3±1.2Ma, whereas hydrothermal mineralization is younger (Late Jurassic/Early Cretaceous; Chen *et al.*, 1996). In the Iberian Massif, W-Mo-Sn quartz veins of the Carris deposit, north Portugal, yield a Re-Os molybdenite age of 279.4±1.2Ma, indicating that circulation of mineralizing fluids took place up to 1–4Ma after the emplacement of the Carris granite (Moura *et al.*, 2014). Thus, although late-Variscan mineralization in part is related to intrusions, in part to hydrothermal veins, it is controlled by the same extensional processes that acted on the large scale.

The late-Variscan ages obtained for the hydrothermal activity at Los Santos and El Cabaco deposits suggest that the W-Au mineralization is younger than the granites of the SCSB and is related to hydrothermal processes along shear zones that became reactivated as the stress field changed during late-Variscan plate reorganization. Actually, available age data indicates that there may also be mineralizing events related to Jurassic and Cretaceous tectonic reactivation of these shear zones (*e.g.* Caballero *et al.*, 1992; Cathelineau *et al.*, 2012; Romer *et al.*, 2010). As these later tectonic events may have resulted in the redistribution of metals within existing deposits, it is quite possible that different stages of mineralization were not related to the same mineralizing event. If these repeated reactivations of old structures occur under contrasting stress regimes, subsequent metal mobilization within a particular deposit may be controlled by different structural elements.

CONCLUSIONS

The integration of mineral assemblages with textural, chemical and age data of uraninite from W-Au mineralization demonstrates their close genetic link with spatially associated granites and multiple metal redistribution during recurrent hydrothermal activity. Using chemical and textural information, uraninite is distinguished into several distinct groups. Uraninite with high contents of Th and REEs, typical of magmatic uraninite, yields a chemical age (300±4Ma) that overlaps with zircon ages of late- to post-Variscan granites from the western part of the SCSB (309 to 303Ma). Hydrothermal uraninite is typically depleted in Th and REEs. It occurs in several different assemblages. Uraninite related to alkali mobilization and early tungsten precipitation yields the oldest ages. Subsequent to this mineralizing phase, the hydrothermal rocks underwent a second event of hydrothermal fluid flux that resulted in uraninite associated with the main stage of tungsten and sulfide deposition and the silicification process in both districts. Uraninites related to this hydrothermal process yield the youngest ages (287±4Ma), which are similar to the ages of the hydrothermal processes recognized at a regional scale. Although the ages of the two hydrothermal uraninite types are not clearly separated, mineral and textural constraints are consistent with the age relation among different uraninite types, *i.e.* old uraninite ages for alkali deposition and young uraninite ages for sulfide, tungsten and silica deposition. Based on mineral assemblages, deposition of gold occurred during this event, but it cannot be dated isotopically. Systematic dating in the Variscan belt of Europe has shown that the late Variscan hydrothermal activity was widespread. Some of these hydrothermal events were not related to magmatic sources, but to high geothermal gradients in an extensional tectonic setting during the Permian reorganization of plate movement. The large time span between hydrothermal activity and magmatism does not reflect a prolonged cooling history of the associated granites but reflects separate thermal events.

ACKNOWLEDGMENTS

This work was supported by Comunidad Autónoma de Castilla y León (Research Projects SA 073/01 and SA015A06) and FEDER program (1FD97-0235). We thank Uwe Dittmann (GFZ) for excellent polished sections from this highly porous material.

REFERENCES

Alexandre, P., Kyser, T.K., 2005. Effects of cationic substitutions and alteration in uraninite, and implications for the dating of uranium deposits. The Canadian Mineralogist, 43(3), 1005-1017.

Antona, F.J., 1991. Fluidos mineralizadores en los yacimientos de oro de Saucelle y El Cabaco (Salamanca). PhD Thesis. University of Salamanca, unpublished, 236pp.

Antona, F.J., Fallick, A.E., García Sánchez, A., 1994. Source of fluids in the auriferous El Cabaco mineralized zone, southern Salamanca. International Geology Review, 36(7), 687-702.

Armstrong, J.T., 1995. CITZAF: A package of correction programs for the quantitative electron microbeam X-ray analysis of thick polished materials, thin films, and particles. Microbeam Analysis, 4(3), 177-200.

Basham, I.R., Easterbrook, G.D., 1977. Alpha-particle autoradiography of geological specimens by use of cellulose nitrate detectors. Transactions of the Institution of Mininig and Metallurgy, Section B, B86, 96-98.

Basham, I.R., 1981. Some application of autoradiography in textural analysis of uranium bearing samples; discussion. Economic Geology, 76(4), 974-982.

Bea, F., Montero, P., Molina, J.F., 1999. Mafic precursors, peraluminous granitoids, and late lamprophyres in the Avila Batolith: a model for the generation of Variscan batoliths in Iberia. The Journal of Geology, 107(4), 399-419.

Bea, F., Villaseca, C., Bellido, F., 2004. El Batolito de Ávila (Sistema Central Español).In: Vera, J.A. (ed.). Geología de España. Sociedad Geológica Española-Instituto Geológico y Minero de España, Madrid, 101-110.

Bowles, J.F.W., 1990. Age dating of individual grains of uraninite in rocks from electron microprobe analyses. Chemical Geology, 83(1-2), 47-53.

Bril, H., Bonhomme, M.G., Marcoux, E., Baubron, J.C., 1991. Ages K/Ar des minéralisations de Brioude-Massiac (W-Au-As-Sb; Pb-Zn), Pontgibaud (Pb-Ag; Sn), et Labessette (As-Pb-Sb-Au): Place de ces districts dans l'évolution géotectonique du Massif central français. Mineralium Deposita, 26(3), 189-198.

Caballero, J.M., Casquet, C., Galindo, C., González-Casado, J.M., Snelling, N., Tornos, F., 1992. Dating hydrothermal events in the Sierra de Guadarrama, Iberian Hercynian Belt, Spain. Geogaceta, 11, 18-22.

Caballero, J.M., Casquet, C., Galindo, C., González-Casado, J.M., Pankhurst, R., Tornos, F., 1993. Geocronología por el método Rb-Sr de las episienitas de la Sierra de Guadarrama. Geogaceta, 13, 16-18.

Caballero, J.M., González-Casado, J. M., Casquet, C., Galindo, C., Tornos, F., 1996. Episienitas de la Sierra de Guadarrama: un proceso hidrotermal regional de edad Pérmico Inferior ligado al inicio de la extensión alpina. Cuadernos de Geología Ibérica, 20, 183-201.

Carnicero, A. (coord.), 1983. Síntesis geológica del Basamento (Zona del centro-oeste español). 1:200,000. Salamanca, Department of Petrology, University of Salamanca.

Casquet, C., Tornos, F., 1984. El skarn de W–Sn del Carro del Diablo (Sistema Central Español). Boletín Geológico y Minero de España, 95(1), 58-79.

Cathelineau, M., Boiron, M.C., Fourcade, S., Ruffet, G., Clauer, N., Belcourt, O., Coulibaly, Y., Banks, D.A., Guillocheau, F., 2012. A major Late Jurassic fluid event at the basin/basement unconformity in western France: $^{40}Ar/^{39}Ar$ and K–Ar dating, fluid chemistry, and related geodynamic context. Chemical Geology, 322-323, 99-120.

Chen, Y., Clark, A.H., Farrar, E., Wasteneys, H.A.H.P., Hodgson, M.J., Bromley, A.V., 1993. Diachronous and independent histories of plutonism and mineralization in the Cornubian Batholith, southwest England. London, Journal of Geological Society, 150, 1183-1191.

Chen, Y., Zentilli, M.A., Clark, A.H., Farrar, E., Grist, A.M., Willis-Richard, J., 1996. Geochronological evidence for post-variscan cooling and uplift of the Carnmenellis granite, SW England. London, Journal of Geological Society, 153, 191-195.

Chesley, J.T., Halliday, A.N., Snee, L.W., Mezger, K., Sheperd, T.J., Scrivener, R.C., 1993. Thermochronology of the Cornubian Batholith in southwest England: implications for pluton emplacement and protracted hydrothermal mineralization. Geochimica et Cosmochimica Acta, 57(8), 1817-1835.

Chicharro, E., Boiron, M.C., López-García, J.A., Barfod, D.N., Villaseca, C., 2016. Origin, ore forming fluid evolution and timing of the Logrosán Sn-(W) ore deposits (Central Iberian Zone, Spain). Ore Geology Reviews, 72, 896-913.

Cuney, M., Alexandrov, P., Carlier, L., de Veslud, C., Cheillez, A., Raimbault, L., Ruffet, G., Scaillet, S., 2002. The timing of W-Sn-rare metals mineral deposit formation in the Western Variscan chain in their orogenic setting: the case of the Limousin area (Massif Central, France). The Journal of the Geological Society of London, 204 (Special Publications), 213-228.

Darbyshire, D.P.F., Shepherd, T.J., 1985. Chronology of granite magmatism and associated mineralization, SW England. The Journal of the Geological Society of London, 142, 1159-1177.

Díaz-Alvarado, J., Fernández, C., Castro, A., Moreno-Ventas, I., 2013. SHRIMP U-Pb zircon geochronology and thermal modeling of multilayer granitoid intrusions: Implications for the building and thermal evolution of the Central System batholith, Iberian Massif, Spain. Lithos, 175-176, 104-123.

Díez Balda, M.A., 1980. La sucesión del Complejo-esquisto-grauváquico al Sur de Salamanca. Estudios Geológicos, 36(1-2), 131-138.

Díez Balda, M.A., 1986. El Complejo Esquisto-Grauváquico, las series paleozoicas y la estructura hercínica al sur de Salamanca. Acta Salmanticensia, Serie Ciencias, 52, 162pp.

Díez Montes, A., 2007. La Geología del Dominio "Ollo de Sapo" en las comarcas de Sanabria y Terra do Bolo. A Coruña, Nova Terra 34, Instituto universitario de geología "Isidro Parga Pondal", Área de xeoloxía e minería do seminario de estudos galegos, 494pp.

Fernández-Suárez, J., Gutiérrez-Alonso, G., Cox, R., Jenner, G.A., 2002. Assembly of the Armorica microplate: a strike-slip terrane delivery? Evidence from U-Pb ages of detrital zircons. The Journal of Geology, 110(5), 619-626.

Finch, R.J., Ewing, R.C., 1992. The corrosion of uraninite under oxidizing conditions. Journal of Nuclear Materials, 190, 133-156.

Finch, R.J., Murakami, T., 1999. Systematics and paragenesis of uranium minerals. In: Burns, P.C., Finch, R. (eds.). Uranium: mineralogy, geochemistry and the environment. Reviews in Mineralogy and Geochemistry, Chantilly (Virginia), Mineralogical Society of America, 91-180.

Finger, F., Waitzinger, M., Förster, H.-J., Kozlik, M., Raith, J.G., 2017. Identification of discrete low-temperature thermal events in polymetamorphic basement rocks using high spatial resolution FE-SEM-EDX U-Th-Pb dating of uraninite microcrystals. Geology, 45(11), 991-994.

Förster, B., Haack, U., 1995. U/Pb-Datierungen von Pechblenden und die hydrothermale Entwicklung der U-Lagerstätte Aue-Niederschlema (Erzgebirge). Zeitschrift für Geologische Wissenschaften, 23, 581-588.

Förster, H.-J., 1999. The chemical composition of uraninite in Variscan granites of the Erzgebirge, Germany. Mineralogical Magazine, 63(2), 239-252.

Förster, H.-J., Tischendorf, G., Trumbull, R.B., Gottesmann, B., 1999. Late-collisional granites in the Variscan Erzgebirge (Germany). Journal of Petrology, 40(11), 1613-1645.

Förster, H.-J., Rhede, D., Stein, H.J., Romer, R.L., Tischendorf, G., 2012. Paired uraninite and molybdenite dating of the Königshain granite: Implications for the onset of late-Variscan magmatism in the Lausitz block. International Journal of Earth Science, 101(1), 57-67.

Frimmel, H.E., Schedel, S., Brätz, H., 2014. Uraninite chemistry as forensic tool for provenance analysis. Applied Geochemistry, 48, 104-121.

Galindo, C., Tornos, F., Darbyshire, D.P.F., 1994. The age and origin of the barite-fluorite (Pb-Zn) veins of the Sierra de Guadarrama (Spanish Central System, Spain): a radiogenic (Nd, Sr) and stable isotope study. Chemical Geology, 112(3-4), 351-364.

González Casado, J.M., Caballero, J.M., Casquet, C., Galindo, C., Tornos, F., 1996. Palaeostress and geotectonic interpretation of the Alpine Cycle onset in the Sierra del Guadarrama (eastern Iberian Central System), based on evidence from episyenites. Tectonophysiscs, 262(1-4), 213-229.

González-Sánchez, M., 2003. Las mineralizaciones de W-As-Au de El Cabaco (Salamanca). Paragénesis, microtermometría y microsonda Raman. Master Thesis. University of Salamanca, unpublished, 100pp.

Gutiérrez-Alonso, G., Fernández-Suárez, J., Collins, A.S., Abad, I., Nieto, E., 2005. Amazonian Mesoproterozoic basement in the core of the Ibero-Armorican Arc: $^{40}Ar/^{39}Ar$ detrital mica ages complement the zircon's tale. Geology, 33(8), 637-640.

Gutiérrez-Alonso, G., Fernández-Suárez, J., Jeffries, T.E., Johnston, S.T., Pastor-Galán, D., Murphy, J.B., Franco, M.P., Gonzalo, J.C., 2011. Diachronous post-orogenic magmatism within a developing orocline in Iberia, European Variscides. Tectonics, 30(5), 17.

Harlaux, M., Romer, R.L., Mercadier, J., Morlot, C., Marignac, C., Cuney, M., 2018. 40 Ma years of hydrothermal W mineralization during the Variscan orogenic evolution of the French Massif Central revealed by U-Pb dating of wolframite. Mineralium Deposita, 53(1), 21-51.

Hazen, R.M., Ewing, R.C., Sverjensky, D.A., 2009. Evolution of uranium and thorium minerals. American Mineralogist, 94(10), 1293-1311.

Janeczek, J., Ewing, R.C., 1992. Structural formula of uraninite. Journal of Nuclear Materials, 190(2), 128-132.

Junta de Castilla y León, 1986. Estudio geológico-minero en el área de la Peña de Francia-Miranda del Castañar (Salamanca). Consejería de Industria, Energía y Trabajo, 188pp+appendices.

Kempe, U., 2003. Precise electron microprobe age determination in altered uraninite: consequences on the intrusion age and the metallogenic significance of the Kirchberg granite (Erzgebirge, Germany). Contributions to Mineralogy and Petrology, 145(1), 107-118.

Kempe, U., Bombach, K., Matukov, D., Schlothauer, T., Hutschenreuter, J., Wolf, D., Sergeev, S., 2004. Pb/Pb and U/Pb zircon dating of subvolcanic rhyolite as a timer marker for Hercynian granite magmatism and Sn mineralization in the Eibenstock granite, Erzgebirge, Germany: considering effects of zircon alteration. Mineralium Deposita, 39(5-6), 646-669.

Keppler, H., Wyllie, P.J., 1990. Role of fluids in transport and fractionation of uranium and thorium in magmatic processes. Nature, 348(6301), 531-533.

Kroner, U., Roscher, M., Romer, R.L., 2016. Ancient plate kinematics derived from the deformation pattern of continental crust: Paleo- and Neo-Tethys opening coeval with prolonged Gondwana-Laurussia convergence. Tectonophysics, 681, 220-233.

López-Moro, F.J., Moro-Benito, M.C., Timón-Sánchez, S.M., 2007. Geochronology of gold deposits associated with Variscan granitoids in central west Iberia. In: Andrew, C.J., Borg, G. (eds.). Digging Deeper: Ninth Biennal Meeting of the Society for Geology Applied to Mineral Deposits. Dublin (Ireland), 20th-23rd August 2007, Proceedings, Irish Association for Economic Geology, 1, 385-388.

López-Moro, F.J., Moro, M.C., Timón, S.M., Cembranos, M.L., Cózar, J., 2013. Constraints regarding gold deposition in episyenites: the Permian episyenites associated with the Villalcampo Shear Zone, central western Spain. International Journal of Earth Sciences, 102(3), 721-744.

López-Moro, F.J., Romer, R.L., López-Plaza, M., González, M., 2017. Zircon and allanite U-Pb ID-TIMS ages of vaugnerites from the Calzadilla Pluton, Salamanca (Spain): Dating mantle-derived magmatism and post-magmatic subsolidus overprint. Geologica Acta, 15(4), 395-408.

Ludwig, K.R., 2003. Isoplot 3.0 - a geochronological toolkit for Microsoft Excel. Special Publication N°4. Berkeley Geochronology Center, Berkeley, California, 71pp.

Marignac, C., Cuney, M., 1999. Ore deposits of the French Massif Central: insight into the metallogenesis of the Variscan collision belt. Mineralium Deposita, 34(5-6), 472-504.

Martín-Crespo, T., Delgado, A., Vindel, E., López-García, J.A., Fabre, C., 2002. The latest Post-Variscan fluids in the Spanish Central System: evidence from fluid inclusión and stable isotope data. Marine and Petroleum Geology, 19(3), 323-337.

Martín-Crespo, T., Vindel, E., López-García, J.A., Cardellach, E., 2004. As-(Ag) sulfide veins in the Spanish Central System: further evidence for a hydrothermal event of Permian age. Ore Geology Reviews, 25(3-4), 199-219.

Moreno-Ventas, I., Rogers, G., Castro, A., 1995. The role of hybridation in the genesis of Hercynian granitoids in the Gredos Massif, Spain: inferences from Sr-Nd isotopes. Contributions to Mineralogy and Petrology, 120(2), 137-149.

Moro Benito, M.C., López-Moro, F.J., Fernández, A., Cembranos, M.L., 2007. Bi-tellurides and sulphosalts in relation with different types of golds from Permian mineralized quartz-veins, El Cabaco area, Spain. In: Andrew, C.J., Borg, G. (eds.). Digging Deeper: Ninth Biennal Meeting of the Society for Geology Applied to Mineral Deposits, Dublin, Ireland 20th–23rd August 2007, Proceedings, Irish Association for Economic Geology, 1, 625-628.

Moura, A., Dória, A., Neiva, A.M.R., Gomes, C.L., Creaser, R.A., 2014. Metallogenesis at the Carris W-Mo-Sn deposit (Gerês, Portugal): constraints from fluid inclusions, mineral geochemistry, Re-Os and He-Ar isotopes. Ore Geology Reviews, 56, 73-93.

Orejana, D., Villaseca, C., Valverde-Vaquero, P., Belousova, E.A., Armstrong, R.A., 2012. U-Pb geochronology and zircon composition of late Variscan S- and I-type granitoids from the Spanish Central System batolith. International Journal of Earth Science, 101(7), 1789-1815.

Pal, D.C., Rhede, D., 2013. Geochemistry and chemical dating of uraninite in the Jaduguda uranium deposit, Singhbhum shear zone India. Implications for uranium mineralization and geochemical evolution of uraninite. Economic Geology, 108(6), 1499-1515.

Plant, J.A., Simpson, P.R., Smith, B., Windley, B.F., 1999. Uranium ore deposits-products of radioactive Echo Bay U-Ni-Ag-Cu deposits, North West Territories, Canada.Economic Geology, 68, 635-656.

Romer, R.L., Schneider, J.C., Linnemann, U., 2010. Post-Variscan deformation and hydrothermal mineralization in Saxo-Thuringia and beyond: a geochronological review. In: Linnemann, U., Romer, R.L. (eds.). Pre- Mesozoic Geology of Saxo-Thuringia – From the Cadomian Active Margin to the Variscan Orogen, Schweizerbart,Stuttgart, 347-360.

Romer, R.L., Thomas, R., Stein, H.J., Rhede, D., 2007. Dating multiply overprinted Sn-mineralized granites–examples form the Erzgebirge, Germany. Mineralium Deposita, 42(4), 337-359.

Romer, R.L., Kroner, U., 2016. Phanerozoic tin and tungsten mineralization-Tectonic controls on the distribution of enriched protoliths and heat sources for crustal melting. Gondwana Research, 31, 60-95.

Steiger, R.H., Jäger, E., 1977. Subcommission on geochronology: Convention on the use of decay constants in geo- and cosmochronology. Earth Planetary Science Letters, 36(3), 359-362.

Timón, S.M., Moro, M.C., 2007. Fluorine concentration in fluids related to the Los Santos scheelite skarn deposit (NW Spain).In: Andrew, C.J., Borg, G. (eds.). Digging Deeper: Ninth Biennal Meeting of the Society for Geology Applied to Mineral Deposits, Dublin, Ireland 20th-23rd August 2007, Proceedings, Irish Association for Economic Geology, 1, 443-446.

Timón, S.M., Moro, M.C., Cembranos, M.L., Fernández, A., Crespo, J.L., 2007. Contact metamorphism in the Los Santos W skarn (NW Spain). Mineralogy and Petrology, 90(1-2), 109-140.

Timón, S.M., 2008. El skarn de scheelita de Los Santos (Salamanca). Química mineral, inclusiones fluidas e isótopos estables. Doctoral Thesis. Universidad de Salamanca, 396pp.

Timón, S.M., Moro, M.C., Cembranos, M.L., 2009. Mineralogical and physiochemical evolution of the Los Santos scheelite skarn, Salamanca, NW Spain. Economic Geology, 104(7), 961-995.

Tornos, F., Casquet, C., Caballero, J.M., 1993. La alteración hidrotermal asociada al Plutón epizonal de Navalcubilla, Sierra de Guadarrama (Sistema Central Español). Revista de la Sociedad Geológica de España, 6(1-2), 67-84.

Tornos, F., Delgado, A., Casquet, C., Galindo, C., 2000. 300 Million years of episodic hydrothermal activity: stable isotope evidence from hydrothermal rocks of the Eastern Iberian Central System. Mineralium Deposita, 35(6), 551- 569.

Tornos, F., Galindo, C., Crespo, J.L., Spiro, B.F., 2008. Geochemistry and origin of calcic tungsten-bearing skarns, Los Santos, Central Iberian Zone, Spain. The Canadian Mineralogist, 46(1), 87-109.

Ugidos, J.M., Rodríguez Alonso, M.D., Albert Colomert, V., Martín Herrero, D., 1990. Explanatory notes of sheet 552 (12-22) (Miranda del Castañar), Geologic map of Spain, 1:50,000. Madrid, Instituto Geológico y Minero de España, 77pp.

Valle Aguado, B., Azevedo, M.R., Schaltegger, U., Martínez Catalán, J.R., Nolan, J., 2005. U-Pb zircon and monazite geochronology of Variscan magmatism related to syn-convergence extension in Central Northern Portugal. Lithos, 82(1-2), 169-184.

Villa, I.M., De Bière, P., Holden, N.E. Renne, P.R., 2015. IUPAC-IUGS recommendation on the half-life of ^{87}R. Geochimica et Cosmochimica Acta, 164(1), 382-385.

Vindel, E., López, J.A., Boiron, M.C., Cathelineau, M., Prieto, A.C., 1995. P-V-T-X-fO_2 evolution from wolframite to sulfides depositional stages in intragranite W-veins. An example from the Spanish Central System. European Journal of Mineralogy, 7(3), 655-673.

Vindel, E., López, J.A., Martín-Crespo, T., García, E., 2000. Fluid evolution and hydrothermal processes of the Spanish Central System. Journal of Geochemical Exploration, 69-70, 359-362.

Votyakov, S.L., Khiller, V.V., Shchapova, Y.V., Erokin, Y.V., 2013. Composition and chemical microprobe dating of U-Th-Bearing minerals. Part 2. Uraninite, thorite, thorianite, coffinite, and monazite from the Urals and Siberia. Geology of Ore Deposits, 55(7), 515-524.

Yenes, M., 1996. Estructura, geometría y cinemática del emplazamiento de los granitoides del área de La Alberca-Béjar (Sistema Central Español, Zona Centro Ibérica). PhD Thesis. University of Salamanca, unpublished, 229pp.

Yenes, M., Álvarez, F., Gutiérrez-Alonso, G., 1999. Granite emplacement in orogenic compressional conditions: the La Alberca-Béjar granitic area (Spanish Central System, Variscan Iberian Belt). Journal of Structural Geology, 21(10), 1419-1440.

Zachariáš, J., Adamović, J., Konečný, P., 2008. The uraninite-pyrite association, a sensitive indicator of changes in paleofluid composition: an example from the Ohre (Eger) Graben, Bohemian Massif, Czech Republic. The Canadian Mineralogist, 46(5), 1159-1172.

Zeck, H.P., Wingate, M.T.D., Pooley, G.D., 2007. Ion microprobe U-Pb zircon geochronology of a late tectonic granitic-gabbroic rock complex within the Hercynian Iberian belt. Geological Magazine, 144(1), 157-177.

Manuscript received February 2018;
revision accepted September 2018;
published January 2019.